Check for updates

ARTICLE

Astrocytes release ATP/ADP and glutamate in flashes via vesicular exocytosis

Heng Li[1,2,3], Yuqing Zhao[1], Ruicheng Dai[4], Peiyao Geng[1,3], Danwei Weng[1], Wenting Wu[1,3], Fengting Yu[4], Rui Lin[1,3], Zhaofa Wu [5], Yulong Li [6,7] and Minmin Luo [4,7,8,9 ✉]

Astrocytes regulate brain functions through gliotransmitters like ATP/ADP and glutamate, but their release patterns and mechanisms remain controversial. Here, we visualized ATP/ADP and glutamate response following astrocyte activation and investigated their mechanisms in vivo. Employing cOpn5-mediated optogenetic stimulation, genetically encoded fluorescent sensors, and two-photon imaging, we observed ATP/ADP released as temporally prolonged and spatially extended flashes that later converted to adenosine. This release occurs via Ca^{2+} and VNUT-dependent vesicular exocytosis. Additionally, astrocytes also release glutamate in flashes through TeNT-sensitive exocytosis, independent of ATP/ADP release. ATP/ADP released by astrocytes triggers further ATP/ADP release from microglia through P2Y12- and VNUT-dependent mechanisms. VNUT in astrocytes and microglia also contributes to ATP/ADP release under LPS-induced brain inflammation. These findings establish Ca^{2+}-dependent vesicular exocytosis as a key mode of action, reveal intricate astrocyte-microglia interactions, and suggest a role for gliotransmission in brain inflammation. Furthermore, the methodologies may provide valuable tools for deciphering glial physiology and pathophysiology.

INTRODUCTION

Astrocytes, the major glial cell type in the central nervous system, exhibit physiological characteristics markedly distinct from those of neurons [1]. Unlike neurons, astrocytes are considered electrically non-excitable, as they do not generate action potentials and lack the synaptic vesicle machinery essential for the rapid release of neurotransmitters [2]. However, astrocytes actively engage in intercellular communication by secreting chemical messengers known as gliotransmitters to interact with nearby neurons, other glial cells, and vascular cells [3, 4]. These gliotransmitters, including amino acids, nucleotides, and peptides, with adenosine triphosphate/adenosine diphosphate (ATP/ADP) and glutamate being particularly notable, play multifaceted roles in modulating neuronal excitation/inhibition balance, synaptic plasticity, and cognitive processes such as learning and memory [5–8]. Gliotransmitters are also increasingly recognized for their roles in the pathogenesis of neuroinflammatory and neurodegenerative diseases [9, 10].

Despite longstanding recognition of gliotransmission, significant gaps persist in our understanding of the patterns and mechanisms of gliotransmitter release in vivo. Conventional methods for stimulating astrocytes—electrical, pharmacological, or mechanical—often lack cellular specificity [11–14]. A critical need in the field is for techniques capable of inducing robust Ca^{2+} signaling in astrocytes, a key mediator of gliotransmitter release [15]. Channel-based optogenetics, instrumental in rapidly modulating neuronal membrane potentials, has transformed neuroscience. While astrocytes exhibit lower excitability, optogenetic stimulation initiates ATP/ADP signaling-related physiological responses [8, 16, 17]. However, traditional optogenetic tools in astrocytes remain sub-optimal, usually causing only a modest increase in intracellular Ca^{2+} signals, approximately 30–50% above baseline levels [18]. Moreover, accurately monitoring the release of specific gliotransmitters like ATP/ADP and glutamate in vivo has been technically challenging. Previous methods, such as 'sniffer cell' approaches, electrophysiological recordings, and microdialysis, have proven inadequate in visualizing gliotransmitters in vivo [19–21]. As a result, the spatiotemporal patterns of ATP/ADP and glutamate release from astrocytes remain elusive. Additionally, the cellular mechanisms of their release are a subject of ongoing debate. Various mechanisms, from Ca^{2+}-dependent vesicular release to non-vesicular release through large-pore membrane channels, have been proposed [13, 22–26]. The occurrence of Ca^{2+}-dependent vesicular exocytosis of ATP/ADP and glutamate from astrocytes in vivo remains contentious [27–29]. Furthermore, the interactions between astrocytes and other glial cells, such as microglia, in shaping gliotransmitter dynamics are not fully understood.

To bridge these gaps, the current study integrates two recently developed methodologies aimed at deciphering gliotransmitter

[1]National Institute of Biological Sciences (NIBS), Beijing, 102206 Beijing, China. [2]School of Life Sciences, Tsinghua University, 100084 Beijing, China. [3]Tsinghua Institute of Multidisciplinary Biomedical Research (TIMBR), 102206 Beijing, China. [4]Chinese Institute for Brain Research (CIBR), Beijing, 102206 Beijing, China. [5]State Key Laboratory of Molecular Developmental Biology, Institute of Genetics and Developmental Biology, Chinese Academy of Sciences, 100101 Beijing, China. [6]State Key Laboratory of Membrane Biology, School of Life Sciences, Peking University, 100871 Beijing, China. [7]New Cornerstone Science Laboratory, 518054 Shenzhen, China. [8]Research Unit of Medical Neurobiology, Chinese Academy of Medical Sciences, 100005 Beijing, China. [9]Beijing Institute for Brain Research, Chinese Academy of Medical Sciences & Peking Union Medical College, 102206 Beijing, China. ✉email: luominmin@cibr.ac.cn

release patterns and mechanisms. Building upon our recent discovery that chicken opsin5 (cOpn5) sensitively responds to light, triggering a strong Ca^{2+} surge in astrocytes via the Gq signaling pathway [30]. we explored its potential for astrocyte activation in vivo. Concurrently, employing genetically encoded sensors $GRAB_{ATP}$ [31] and iGluSnFR [32, 33] for ATP/ADP and glutamate, respectively, we visualized real-time release dynamics through two-photon imaging. Our results demonstrate robust ATP/ADP and glutamate release from astrocytes upon extended optogenetic stimulation, manifesting as large, discrete flashes lasting tens of seconds. Crucially, these releases are mediated by Ca^{2+}-dependent exocytotic pathways, with ATP/ADP specifically requiring the vesicular nucleotide transporter (VNUT). Notably, astrocyte-derived ATP/ADP stimulates further ATP/ADP release from microglia through P2Y12- and VNUT-dependent exocytosis, thereby highlighting a previously unappreciated role for microglia in amplifying gliotransmitter signaling. Under LPS-induced brain inflammation, both astrocytes and microglia exhibited VNUT-dependent ATP/ADP release. These findings illuminate the unique features and mechanisms of gliotransmitter releases by astrocytes and suggest potential roles for ATP/ADP in mediating astrocyte-microglia interactions during brain inflammation. Moreover, the methodologies developed herein offer valuable tools and paradigms for further exploration of the complex interactions between glial cells and neurons.

RESULTS

cOpn5 optogenetics elicits dynamic Ca^{2+} signals in cortical astrocytes in vivo

To activate cortical astrocytes, we first utilized the neuropsin-based optogenetic tool cOpn5, which triggers the Gq protein signaling pathway in response to single-photon blue light [30]. To address its suitability for in vivo applications using two-photon light, we delivered pulsed femtosecond laser light to cOpn5-expressing HEK 293T cells and monitored the changes in fluorescence of the red Ca^{2+}-sensitive dye Calbryte 630 (Supplementary Fig. S1a). This approach revealed that 850–920 nm two-photon light pulses rapidly elicited Ca^{2+} transients at an intensity comparable to that typically used for in vivo two-photon imaging (Supplementary Fig. S1b, c). Based on these observations, we chose 920 nm two-photon light for simultaneous excitation of cOpn5 and imaging with GFP-based fluorescent indicators in vivo.

To elucidate the functional response of cortical astrocytes to cOpn5-mediated optogenetic stimulation, we co-expressed the Ca^{2+} indicator GCaMP6s with cOpn5 in astrocytes within the primary somatosensory cortex (S1) of mice. This was achieved through infusing adeno-associated viruses (AAVs) carrying the GCaMP6s or cOpn5-T2A-mCherry construct, under the control of the GfaABC1D promoter, into the mouse S1. Immunohistochemistry confirmed the selective expression of mCherry, bicistronically expressed along with cOpn5, in astrocytes, but not in neurons or microglia (Supplementary Fig. S1d, e).

We examined GCaMP fluorescent changes using two-photon microscopy through an acutely implemented cranial window over the S1 cortical area of anesthetized mice (Fig. 1a, b). Pulsed 920 nm laser for imaging elicited a rapid elevation in intracellular Ca^{2+} signals from cOpn5-expressing astrocytes, but not from mCherry-expressing control astrocytes (Fig. 1c; Supplementary video 1). This increase in Ca^{2+} signals commenced within 1-2 s, reaching a peak approximately 10 s post-stimulation (Fig. 1d; Supplementary video 1). Ca^{2+} signals in astrocytes were activated reproducibly in multiple sessions of 5-minute activation and 5-minute recovery (Supplementary Fig. S1f–h), demonstrating the capability of cOpn5 for mediating reliable optogenetic activation of astrocytes. Furthermore, the peak activation was followed by persistent oscillations and wave-like patterns within the astrocyte network, enduring throughout the 60-min imaging session under

continuous two-photon light for imaging and activation (Fig. 1c, Supplementary Fig. S1i, j). The selective Gq pathway antagonist YM-254890 abolished the Ca^{2+} signals in cOpn5-expressing astrocytes (Fig. 1c–e), thereby substantiating that cOpn5 facilitates the in vivo activation of astrocytes via the Gq-signaling pathway.

We also explored two additional tools tailored to stimulate astrocytes. Chemogenetic approaches, including designer receptors exclusively activated by designer drugs (DREADDs), are commonly employed to activate specific G-protein signal pathways in astrocytes [34]. After expressing GCaMP6s and the Gq-coupled hM3Dq in astrocytes (Supplementary Fig. S2a), administration of the designer drug clozapine N-oxide (CNO, 2 mg/kg; i.p.) led to a rise in Ca^{2+} signals, which reached a peak within five minutes and remained elevated for at least 30 minutes post-peak (Supplementary Fig. S2b, c) [35]. In contrast to cOpn5 optogenetics, chemogenetic activation via hM3Dq primarily generated sustained Ca^{2+} signals in the somata without exhibiting significant temporal dynamics (Supplementary Fig. S2b–e). Additionally, stimulating Gi signaling is thought to enhance Ca^{2+} signals in astrocytes [35, 36] eOpn3, a targeted mosquito homolog of vertebrate encephalopsin, is coupled to the Gi-pathway and inhibits neuronal activity [37, 38]. Upon co-expression of GCaMP6s and eOpn3 in astrocytes (Supplementary Fig. S3a), continuous two-photon laser stimulation rapidly elevated astrocyte Ca^{2+} signals, which then significantly decreased within two minutes (Supplementary Fig. S3b, c).

Collectively, our findings indicate that optogenetic techniques utilizing cOpn5 and eOpn3, along with the chemogenetic approach via hM3Dq, enhance Ca^{2+} signaling in astrocytes. Notably, the cOpn5 method generates robust and dynamic Ca^{2+} signals that persist over extended durations.

cOpn5 optogenetic activation of cortical astrocytes evokes strong ATP/ADP release

Next, we focused on gliotransmission induced by astrocyte activation. Prior studies have established the roles of ATP/ADP release by astrocytes in modulating brain functions [8, 39, 40]. However, direct visualization using fluorescence sensors and in vivo analysis of ATP/ADP release mechanisms following astrocytic activation remained unexplored. To determine whether Gq signaling activation in astrocytes triggers ATP/ADP release, we co-expressed $GRAB_{ATP1.0}$, a recently developed GPCR activation-based sensor characterized by a robust fluorescence response to extracellular ATP/ADP [31], with cOpn5 in astrocytes via AAV vectors (Fig. 1f, g). In the S1 region of anesthetized mice, we observed no discernible $GRAB_{ATP1.0}$ signals within the initial 2–3 min of two-photon imaging and activation. Subsequently, sustained optogenetic stimulation of cOpn5-expressing astrocytes induced discrete distinct fluorescent flashes that progressively intensified in frequency, reaching a peak between 6–8 min and persisting throughout the entire 20-min imaging period. (Fig. 1h; Supplementary video 2). We overcame the limitations of traditional ROI-based methods by utilizing the Astrocyte Quantitative Analysis (AQuA) algorithm, an event-based detection methodology [41], to analyze spatially heterogeneous, size-varying, and propagative ATP/ADP fluorescent flashes, characterizing them as individual release events and quantifying these events per imaging area. This analysis revealed ~35 ATP/ADP release events per $100 \times 100 \, \mu m^2$ over the 20-min activation period with co-expression of cOpn5 and the ATP/ADP sensor, while the control group lacking cOpn5 expression displayed only about 0.2 ATP/ADP release events within the same spatiotemporal range (Fig. 1i–k).

ATP/ADP flashes typically emerged as small spots about ten μm in diameter, expanded over approximately 10 s, and gradually faded within 60 s (Fig. 1l). Considering the rapid sensor kinetics of $GRAB_{ATP1.0}$ [31], the protracted temporal features of ATP/ADP flashes suggest a sustained engagement of membrane-bound
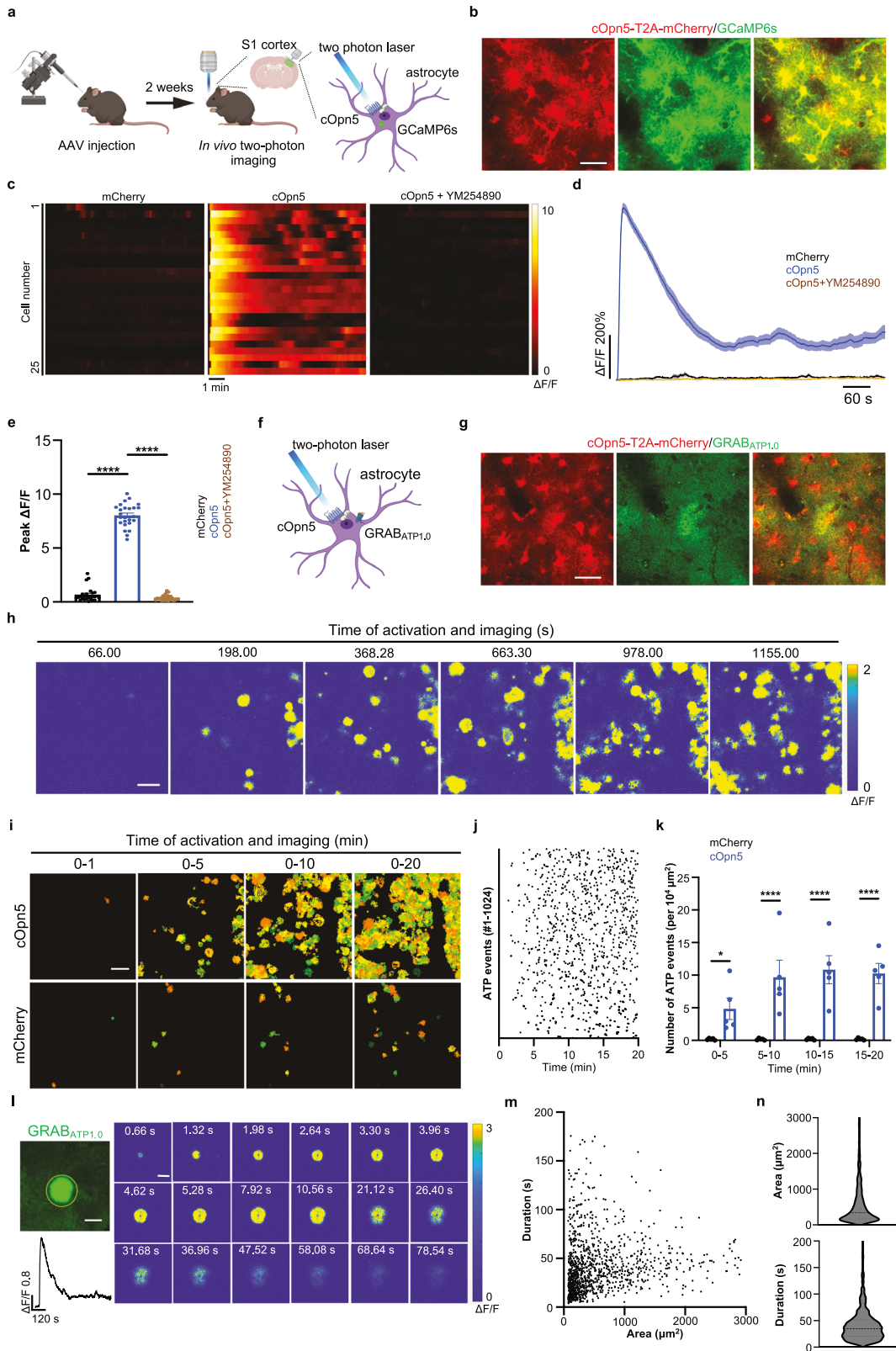
ATP/ADP receptors, along with processes involving the diffusion and clearance of extracellular ATP/ADP. Among the thousands of ATP/ADP release events observed, the fluorescent flashes varied in size from one hundred to thousands μm^2 (median 326 μm^2, 1st quartile 158 μm^2, 3rd quartile 770 μm^2) and in duration from a few seconds to over one hundred seconds (median 33 s, 1st quartile

19 s, 3rd quartile 50 s; Fig. 1m, n), implying the potential of each ATP/ADP flash to affect multiple neighboring cells across diverse time scales.

Activation of astrocytes via Gq-coupled DREADDs did not efficiently elicit ATP/ADP release (Supplementary Fig. S2f–h). Activation of Gi signaling in astrocytes using eOpn3 optogenetics

Fig. 1   cOpn5 optogenetics elicits Ca^{2+} signals in cortical astrocytes and prompts ATP/ADP release. a Schematic of the protocol for two-photon activation and Ca^{2+} imaging of astrocytes in vivo. **b** Representative images depicting AAV-mediated bicistronic expression of cOpn5 and mCherry (red) alongside GCaMP6s expression (green) in astrocytes. Scale bar, 40 μm. **c** Heatmap representation of Ca^{2+} signals within individual astrocytes expressing either mCherry alone (left) or cOpn5 (middle and right), with or without the Gq protein inhibitor YM254890 ($n = 25$ cells per group). **d** Time-course traces of Ca^{2+} signals in astrocyte populations expressing either mCherry alone (control, black), cOpn5 (blue), or cOpn5 with YM254890 treatment (brown). Each trace represents the average of cells per group. **e** Quantitative group data for peak Ca^{2+} signals (ΔF/F) comparing the mCherry-only control group with cOpn5-expressing groups, with or without YM254890 ($n = 25$ cells per group; unpaired t-tests). **f** Overview of the experimental strategy for optogenetic stimulation and ATP/ADP imaging of astrocytes, featuring co-expression of cOpn5 and the ATP/ADP sensor GRAB$_{ATP1.0}$ via separate AAV vector delivery. **g** Two-photon microscopy images showing bicistronic expression of cOpn5 and mCherry (red) and a snapshot of GRAB$_{ATP1.0}$ signals (green) in astrocytes. Scale bar, 40 μm. **h** Pseudocolor series of GRAB$_{ATP1.0}$ fluorescence images at distinct time points following cOpn5 activation. Scale bar, 100 μm. **i** Pseudocolor images showing accumulative ATP/ADP flash events in astrocytes expressing cOpn5 (upper) or mCherry alone (control, lower). Scale bar, 100 μm. **j** Dot plots indicating the temporal occurrence of individual ATP/ADP flash events. **k** Aggregate data displaying the cumulative number of ATP/ADP flash events normalized to the field of view area at 5-minute intervals over 20 min of cOpn5 activation ($n = 5$ mice per group; two-way ANOVA). **l** An individual ATP/ADP release event, comprising a time trace from a region of interest (ROI; left) and ΔF/F0 pseudocolor images (right) at specified time points. Scale bar, 30 μm. **m** Scatter Plot delineating the area and duration of individual ATP/ADP release events induced by cOpn5 activation ($n = 1162$ events). **n** Violin plots illustrating the distribution of the area and duration of single ATP/ADP release events induced by cOpn5 activation ($n = 1162$ events). Dashed horizontal lines represent the first quartile, median, and third quartile. In **e** and **k**, error bars indicate SEM, ns, $p > 0.05$; *$p < 0.05$; ****$p < 0.0001$. See Supplementary Table S1 for detailed information about inferential statistical tests.

also evoked clear ATP/ADP release (Supplementary Fig. S3d–h), albeit in a substantially lesser amount than cOpn5 optogenetic activation of Gq signaling in astrocytes (Fig. 1i–k). These findings demonstrate that cOpn5-mediated optogenetics is the most effective among the three tools evaluated for investigating ATP/ADP release subsequent to astrocyte activation.

The observed gradual fading of ATP/ADP flashes is likely due to extracellular hydrolysis. Adenosine (ado), a well-established product of extracellular ATP/ADP enzymatic breakdown, plays multifaceted roles as an important brain signaling molecule (Supplementary Fig. S4a) [17, 42–44]. To explore whether astrocyte activation elevates extracellular adenosine levels and to elucidate the underlying mechanisms, we introduced a genetically encoded GPCR activation-based adenosine fluorescent sensor with medium affinity, GRAB$_{Ado1.0m}$ [42, 44], into neurons surrounding cOpn5-expressing astrocytes (Supplementary Fig. S4a, b). Upon astrocytic activation for 2-3 min, we detected a strong increase in extracellular adenosine signals (Supplementary Fig. S4c; Supplementary video 3). Initially, these adenosine signals manifested as discrete fluorescence flashes, similar in size and duration to those of ATP/ADP (Supplementary Fig. S4d). However, unlike the ATP/ADP flashes, the adenosine signals were more diffuse and became indistinct as individual events, particularly when they accumulated in substantial quantities (Supplementary Fig. S4c, d). Approximately ten minutes into the imaging session, the prevalence of these signals started to decrease, likely a result of sensor saturation and/or desensitization (Supplementary Fig. S4c). In the control group, only a few sporadic adenosine signals were observed (Supplementary Fig. S4e). Notably, the genetic elimination of CD73, a major ectoenzyme within the pathway for converting extracellular ATP/ADP into adenosine [43], abolished the adenosine signal following astrocytic activation (Supplementary Fig. S4e–g). These results collectively demonstrate that Gq signaling in astrocytes induces an increase in extracellular adenosine levels. This increase is not due to direct release but rather results from the extracellular hydrolysis of ATP/ADP.

ATP/ADP is released through VNUT-dependent exocytosis
Astrocytes are known to release ATP/ADP via either Ca^{2+}-dependent vesicular exocytosis or non-vesicular mechanisms, such as through the channel opening of pannexin [45, 46]. Results from several experiments revealed that optogenetic activation of astrocyte Gq signaling leads to Ca^{2+}-dependent vesicular exocytosis of ATP/ADP. Firstly, ATP/ADP release induced by optogenetic stimulation of astrocytes was fully blocked by the Gq protein inhibitor YM-254890 and the cell-permeable Ca^{2+} chelator BAPTA-AM, indicating a reliance on Gq signaling and Ca^{2+} (Fig. 2a, b; Supplementary Fig. S5a, b). Secondly, the ATP/

ADP release was markedly reduced by the vacuolar H$^+$-ATPase inhibitor bafilomycin A1 (BafA1), which pointed to a vesicular release mechanism (Fig. 2a, b). In contrast, inhibition of pannexin-1 channels with probenecid (PBN) did not impact ATP/ADP release (Fig. 2a, b). Furthermore, tetrodotoxin (TTX), which inhibits neuronal firing by blocking several Na$^+$ channels, failed to reduce ATP/ADP release (Fig. 2a, b; Supplementary Fig. S5c–e), indicating that astrocyte activation-induced ATP/ADP release is independent of action potential-dependent neuronal activity.

Thirdly, we disrupted exocytosis by expressing the light chain of tetanus toxin [TeNT (LC)] in astrocytes. This protein cleaves synaptobrevin-2, a crucial V-SNARE necessary for vesicle fusion to the membrane [47]. Astrocytes expressing TeNT (LC) exhibited significant inhibition of ATP/ADP release compared to those expressing the protease-inactive TeNT (LC, E234A) [48] and to neurons expressing TeNT (LC) (Fig. 2c–e), demonstrating that vesicular docking in astrocytes is crucial for ATP/ADP release post-activation. We noted that the expression of TeNT (LC) in neurons did not affect the frequency and duration of ATP/ADP release events, but produced significantly smaller flashes (Fig. 2f), suggesting a potential effect on the diffusion, hydrolysis, or reuptake of extracellular ATP/ADP.

Most importantly, we investigated the role of the vesicular transporter of ATP/ADP. Solute carrier family 17, member 9 (SLC17A9)/vesicular nucleotide transporter (VNUT), has been identified as crucial for actively accumulating ATP/ADP into vesicles (Supplementary Fig. S6a) [49], and is implicated in ATP/ADP exocytosis in astrocytes [50, 51]. To assess whether ATP/ADP release is VNUT-dependent, we generated *Slc17a9* knockout (KO) mice using CRISPR-Cas9 (Supplementary Fig. S6b). We validated the efficiency of *Slc17a9* knockout at the genomic and RNA levels by mouse genome sequencing, Reverse Transcription-Quantitative Real-time PCR (RT-qPCR), and Single Molecule Fluorescent In Situ Hybridization (smFISH) (Supplementary Fig. S6c–f). The knockout of *Slc17a9* almost completely halted ATP/ADP release, with only a few events remaining (Fig. 2g, h).

Collectively, these findings underscore that ATP/ADP is released through a VNUT-dependent and TeNT-sensitive exocytosis machinery upon the activation of Gq signaling in astrocytes.

Astrocytes release glutamate via TeNT-sensitive exocytosis
Previous studies indicate the release of ATP/ADP and glutamate from astrocytes differentially modulate synaptic physiology [21, 52]. However, direct comparisons of the release patterns of ATP/ADP and glutamate have not yet been conducted. To investigate glutamate release upon Gq signaling activation in astrocytes, we expressed cOpn5 and a GFP-based intensiometric glutamate reporter (SF-iGluSnFR) in astrocytes and neurons,
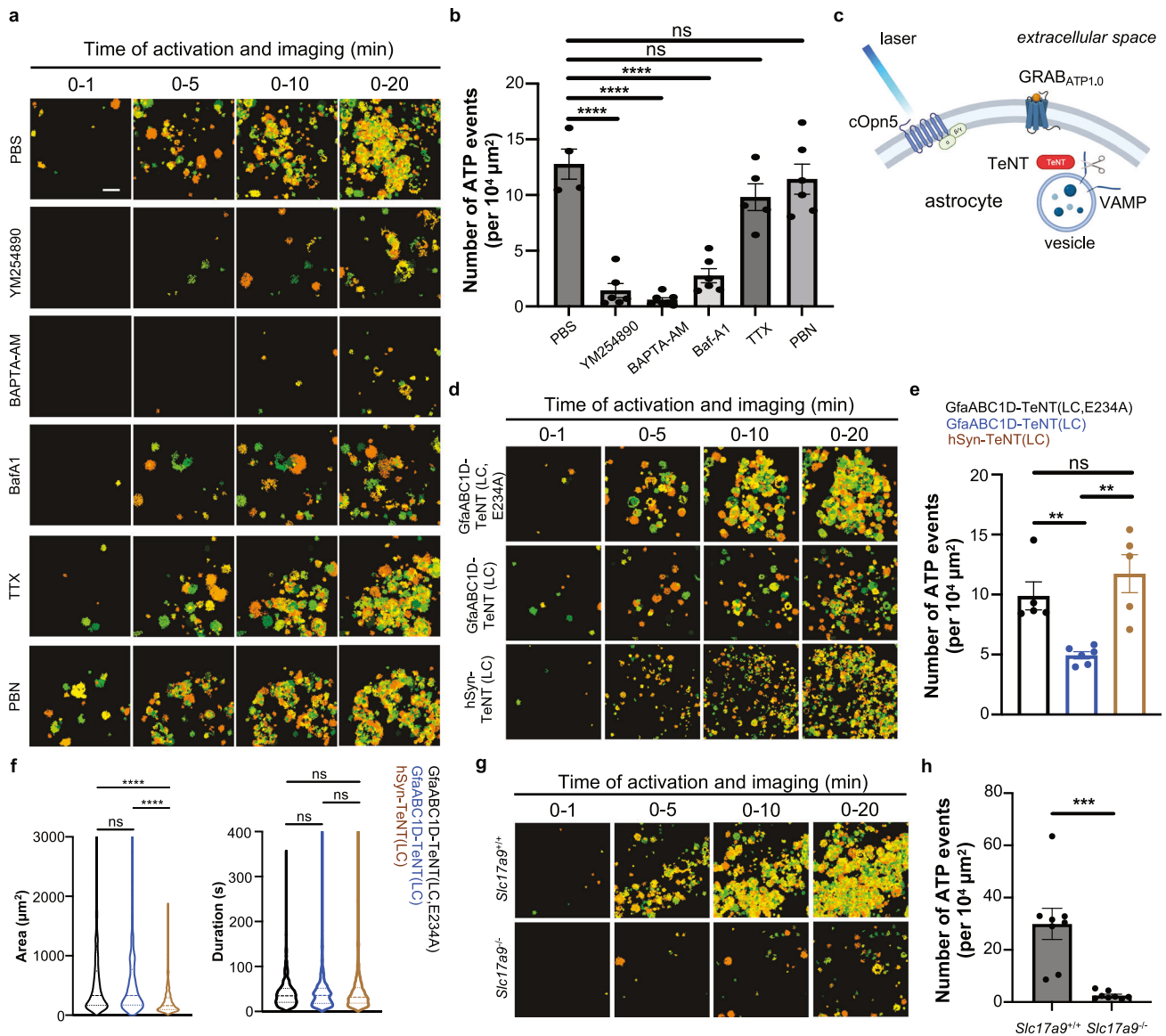
Fig. 2 **ATP/ADP release occurs via VNUT-dependent vesicular exocytosis.** Representative images (**a**) and group data (**b**) showing ATP/ADP-release events within 20 min of light activation following intracerebral infusions of PBS control ($n = 4$ mice), YM254890 ($n = 6$ mice), BAPTA-AM (membrane permeable Ca^{2+} chelator; $n = 7$ mice), BafA1 (vacuolar H^+-ATPase inhibitor; $n = 6$ mice), TTX (Na^+ channel inhibitor; $n = 5$ mice), or PBN (pannexin-1 channel blocker; $n = 6$ mice). Statistical comparisons were made using unpaired t-tests. Scale bar in **a**, 100 μm. **c** Diagrammatic representation of the experimental strategy for AAV-mediated expression of cOpn5, GRAB$_{ATP1.0}$, and either TeNT (light chain; LC) or inactive TeNT (LC, E234A) in astrocytes or neurons. Representative images (**d**) and group data (**e**) showing ATP/ADP-release events in TeNT- or inactive TeNT(E234A)-expressing mice ($n = 5$ mice for GfaABC1D-TeNT (E234A) group, 6 mice for GfaABC1D-TeNT group, and 5 mice for hSyn-TeNT group). Unpaired t-tests. **f** Violin plots detailing the distribution of the area and duration of single ATP/ADP release events in TeNT-expressing groups ($n = 1147$ events for GfaABC1D-TeNT (E234A) group, 681 events for GfaABC1D-TeNT group, and 643 events for hSyn-TeNT group). Horizontal dashed lines indicate the first quartile, median, and third quartile. Mann–Whitney U test. Representative images (**g**) and comparative group data (**h**) showing ATP/ADP-release events in WT or VNUT/Slc17a9 knockout mice ($n = 8$ mice per group). Unpaired t-tests. Error bars in **b**, **e**, and **h** indicate SEM. ns, $p > 0.05$; **$p < 0.01$; ***$p < 0.001$; ****$p < 0.0001$. See Supplementary Table S1 for detailed information about inferential statistical tests.

respectively (Fig. 3a, b) [32, 33]. Optogenetic activation of astrocytes resulted in notable glutamate release, manifested as individual fluorescence flashes that began with an approximate one-minute delay, peaked around 6–8 min, and persisted throughout the imaging session (Fig. 3c–e; Supplementary video 4). Using the AQUA algorithm, we identified 5-6 glutamate release events per 10^4 μm imaging area over ten minutes of activation and imaging (Fig. 3f). In control groups with astrocytes expressing only mCherry, no glutamate release events were detected (Fig. 3f). In contrast to the effectiveness of cOpn5-mediated optogenetics, Gq-coupled DREADD activation of

astrocytes induced minimal glutamate release (Supplementary Fig. S2i–k). Gi signaling activation via eOpn3 optogenetics triggered glutamate release, but the event frequency was only one-fourth that of cOpn5 optogenetic activation (Fig. 3f; Supplementary Supplementary Fig. S3g–j). Thus, we focused on using cOpn5 to further investigate the pattern and mechanisms of glutamate release in response to astrocyte activation.

Individual glutamate release events presented as swiftly emerging spots with minimal fluorescent flash areas, expanding within ~5 s and vanishing within ~10 s (Fig. 3g). The fluorescence flash areas of these glutamate events were mostly less than
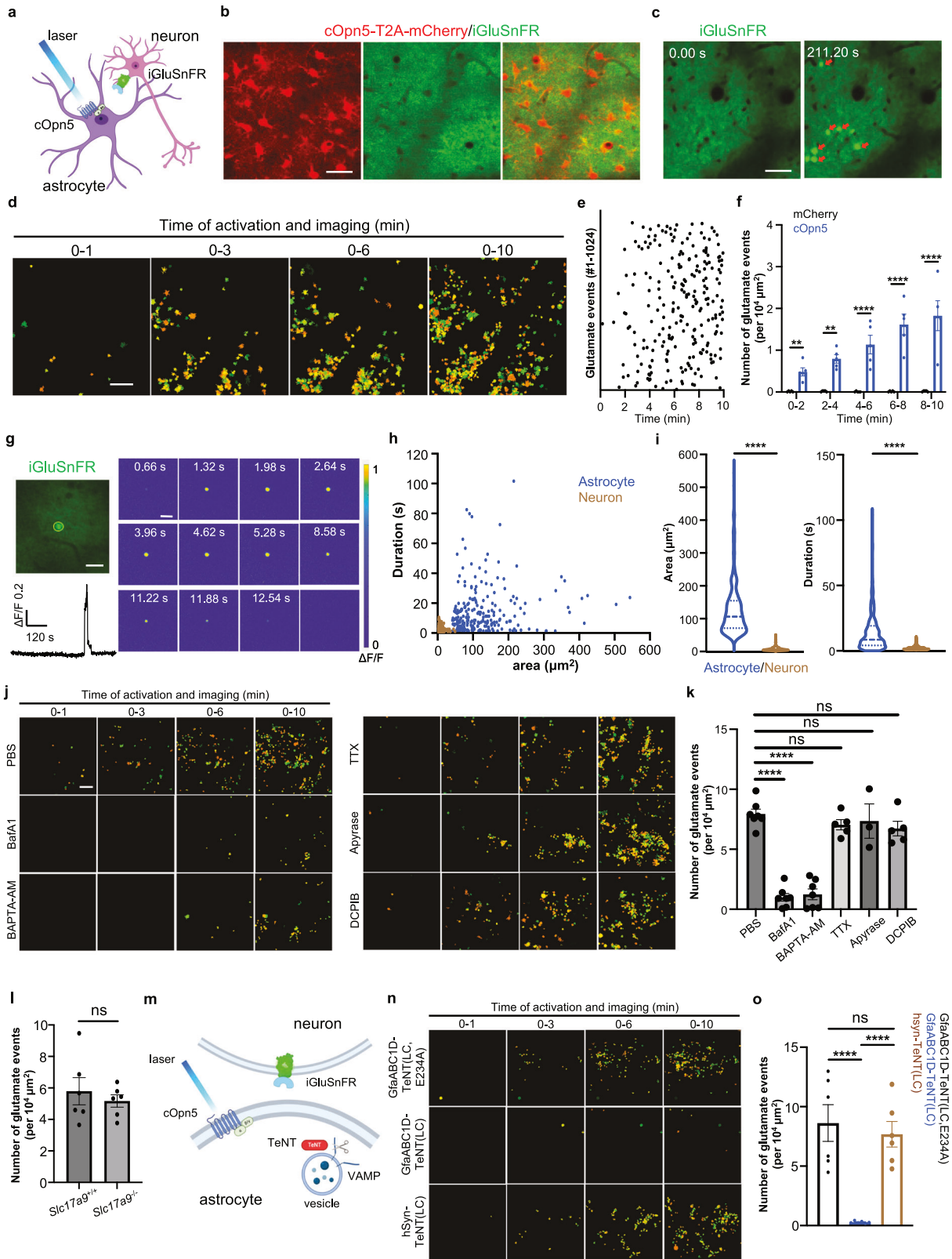
200 μm² (median 102 μm², 1st quartile 68 μm², 3rd quartile 151 μm²) and lasted up to 50 s (median 8 s, 1st quartile 3 s, 3rd quartile 18 s; Fig. 3h, i). Hence, glutamate flashes are typically more transient and smaller than ATP/ADP flashes (Fig. 1l, n), suggesting distinct mechanisms for their release or removal.

We also examined the differences between astrocyte-induced glutamate release and synaptic glutamate release from neurons. To monitor synaptic glutamate release in awake mice, we employed the advanced iGluSnFR3, known for its rapid and nonsaturating activation kinetics (Supplementary Fig. S7a) [53].

Fig. 3 Astrocytes release glutamate through TeNT-sensitive exocytosis. a Diagrammatic representation of the experimental methodology. AAV vectors were used to express cOpn5 in astrocytes and the glutamate sensor iGluSnFR in neurons. **b** Two-photon microscopy images exemplifying bicistronic expression of cOpn5 and mCherry (red) within astrocytes and separate iGluSnFR expression (green) in neurons. Scale bars, 40 μm. **c** Representative two-photon microscopy images depicting iGluSnFR fluorescence at designated time points. Red arrows highlight glutamate-release events triggered by cOpn5 activation. Scale bars, 40 μm. **d** Images showcasing cumulative glutamate-release events induced by cOpn5 activation at specified time intervals. Scale bar, 100 μm. **e** Dot plots tracking the incidence of individual glutamate flash events over time. **f** Group data showing the cumulative number of glutamate flash events normalized to the field of view area, for every two minutes over a 10-min period of cOpn5 activation ($n = 5$ mice per group). Two-way ANOVA. **g** Depiction of a singular glutamate release event, encompassing a time trace derived from a region of interest (ROI, left) and ΔF/F pseudocolored images (right). Scale bar, 30 μm. Scatter Plot (**h**) and violin plots (**i**) delineating the distribution of area and duration of individual glutamate release events elicited by astrocyte activation (blue; $n = 232$ events) and spontaneous neuronal activity (brown; $n = 356$ events) as detected independently by SF-iGluSnFR and iGluSnFR3. Horizontal dashed lines in **i** indicate the first quartile, median, and third quartile. Mann–Whitney U test. **j** Representative images illustrating cumulative glutamate-release events at the specified time points post-intracerebral infusions of PBS (vesicle control), BafA1, BAPTA-AM, TTX, Apyrase, or DCPIB. Scale bar, 100 μm. **k** Comparative group data quantifying glutamate-release events following pretreatment with various pharmacological agents ($n = 6$ mice for PBS, 7 mice for BafA1, 7 mice for BAPTA-AM, 5 mice for TTX, 3 mice for apyrase, and 5 mice for DCPIB). Unpaired t-tests. **l** Group data illustrating the number of glutamate release events over 10 min in wild-type (WT) or slc17a9 KO mice ($n = 6$ mice for each group). Unpaired t-tests. **m** Schematic outline of the experimental strategy for AAV-mediated expression of cOpn5, iGluSnFR, TeNT, and inactive TeNT (E234A) targeted to astrocytes or neurons. Representative images (**n**) and group data (**o**) showing the number of glutamate-release events in TeNT or the inactive TeNT(E234A)-expressing mice ($n = 6$ mice per group; unpaired t-tests). Error bars in **f**, **k**, **l**, and **p** indicate SEM. ns, $p > 0.05$; **$p < 0.01$; ****$p < 0.0001$. See Supplementary Table S1 for detailed information about inferential statistical tests.

This sensor revealed numerous spontaneous glutamate fluorescence transients, predominantly hundreds of milliseconds in duration and with diameters of 1-2 μm, limited by imaging resolution (Supplementary Fig. S7b, c). Interestingly, a small subset of these signals persisted for about ten seconds and exceeded 5 μm in diameter, mirroring the glutamate dynamics induced by astrocytes as observed with SF-iGluSnFR (Fig. 3g–i; Supplementary Fig. S7b, c). A comparison of duration and area between spontaneous neuronal glutamate release and astrocyte-induced release showed marked differences, with astrocyte-induced events exhibiting much larger areas and longer durations (Fig. 3h, i), thus implying different mechanisms of astrocyte gliotransmission and neurotransmission.

We performed several experiments to elucidate the mechanism underlying glutamate release. Pretreatment with the vacuolar H^+-ATPase inhibitor Bafilomycin A1 (BafA1) and the Ca^{2+}-chelator BAPTA-AM significantly decreased the number of glutamate release events, whereas inhibiting action potential firing with TTX and blocking volume-regulated anion channels with DCPIB had no effect (Fig. 3j, k). Furthermore, introducing the light chain of tetanus toxin [TeNT (LC)] into astrocytes, which disrupted vesicular release of ATP/ADP, also abolished glutamate release, in contrast to controls using protease-inactive TeNT (LC, E234A) and neurons expressing TeNT (LC) (Fig. 3m–o). These results indicate that glutamate release from activated astrocytes is mediated via Ca^{2+}-dependent exocytosis.

Subsequent experiments established that astrocytic glutamate release occurs independently of ATP/ADP release. The intracerebral administration of apyrase, an ATP-diphosphohydrolase, did not suppress glutamate release (Fig. 3j, k). Additionally, glutamate release from activated astrocytes was resilient to VNUT knockout (Fig. 3l), indicating independence from VNUT-dependent ATP/ADP release and microglial activity.

Microglia amplify ATP/ADP released by astrocytes
Microglia, another major glial cell type in the brain, are morphologically and functionally intertwined with astrocytes [54]. However, how astrocytic activation recruits microglia in the process of gliotransmission is not well understood. We first investigated the functional and morphological responses of microglia in vivo following optogenetic activation of astrocytes. To monitor microglial Ca^{2+} signaling, we employed AAV vectors to express cOpn5 in astrocytes of mice that also expressed GCaMP6s specifically in microglia (Cx3cr1-CreER^T2::GCaMP6s) (Fig. 4a, b). Optogenetic activation of astrocytes resulted in a significant increase in microglial Ca^{2+} signals, with a delayed onset of

approximately 1–2 min and lasting throughout the imaging session (Fig. 4c, d; Supplementary video 5). In control groups, where astrocytes expressed only mCherry, microglia displayed infrequent Ca^{2+} transients, consistent with previous studies indicating that resting microglia are typically quiescent (Fig. 4c, d) [55]. Furthermore, in line with existing knowledge that activated microglia undergo distinct morphological changes [56], two-photon imaging in Cx3cr1-GFP mice revealed that microglia adopted an "amoeba-like" activated morphology, characterized by larger soma areas and reduced surveillance areas, following persistent light activation of cOpn5-expressing astrocytes (Supplementary Fig. S8a, b). These findings suggest that astrocyte activation triggers corresponding changes in microglial activation status, underscoring a significant functional interconnection between these two glial cell types.

Given the capacity of microglia to release ATP/ADP [57], we hypothesized their involvement in gliotransmission following astrocyte activation. Using BLZ945, an inhibitor of the colony-stimulating factor-1 receptor (CSF-1R) [58], we depleted microglia and observed a significant reduction, confirmed by Iba1 immunostaining, nine days post-treatment (Fig. 4e; Supplementary Fig. S8c, d). Subsequent in vivo two-photon imaging revealed that microglial ablation significantly reduced ATP/ADP release (Fig. 4f, g), but not glutamate release (Fig. 4h), upon astrocytic activation, suggesting a role for microglia in ATP/ADP release.

Combining smFISH of Slc17a9 with immunohistochemical staining revealed Slc17a9 expression in both astrocytes and microglia (Fig. 4i). To decipher microglial involvement in ATP/ADP release, we generated mutant mice with conditional knock-out of VNUT either in astrocytes or microglia, by crossing VNUT-floxed (Slc17a9^fl/fl) mice with transgenic mice bearing a tamoxifen-inducible Cre recombinase under the control of an aldehyde dehydrogenase 1 family member L1(Aldh1l1) promoter/enhancer regions [59] (Aldh1l1-CreER^T2::Slc17a9^fl/fl) or Cx3cr1 promoter/enhancer elements (Cx3cr1-CreER^T2::Slc17a9^fl/fl) (Supplementary Fig. S6g). Conditional Slc17a9 knockout was confirmed at the mRNA level (Supplementary Fig. S6h). Both conditional knockout lines exhibited a significantly decreased number of ATP/ADP events in response to optogenetic activation of astrocytes, with the reduction being more pronounced in astrocyte-specific knockout (Fig. 4j, k).

These cell-type-specific VNUT knockout experiments suggest a collaborative mechanism in gliotransmission: astrocytes initiate ATP/ADP release, while microglia amplify extracellular ATP/ADP signals through an ATP/ADP-induced process. Microglia sense extracellular ATP/ADP through various purinergic receptors,
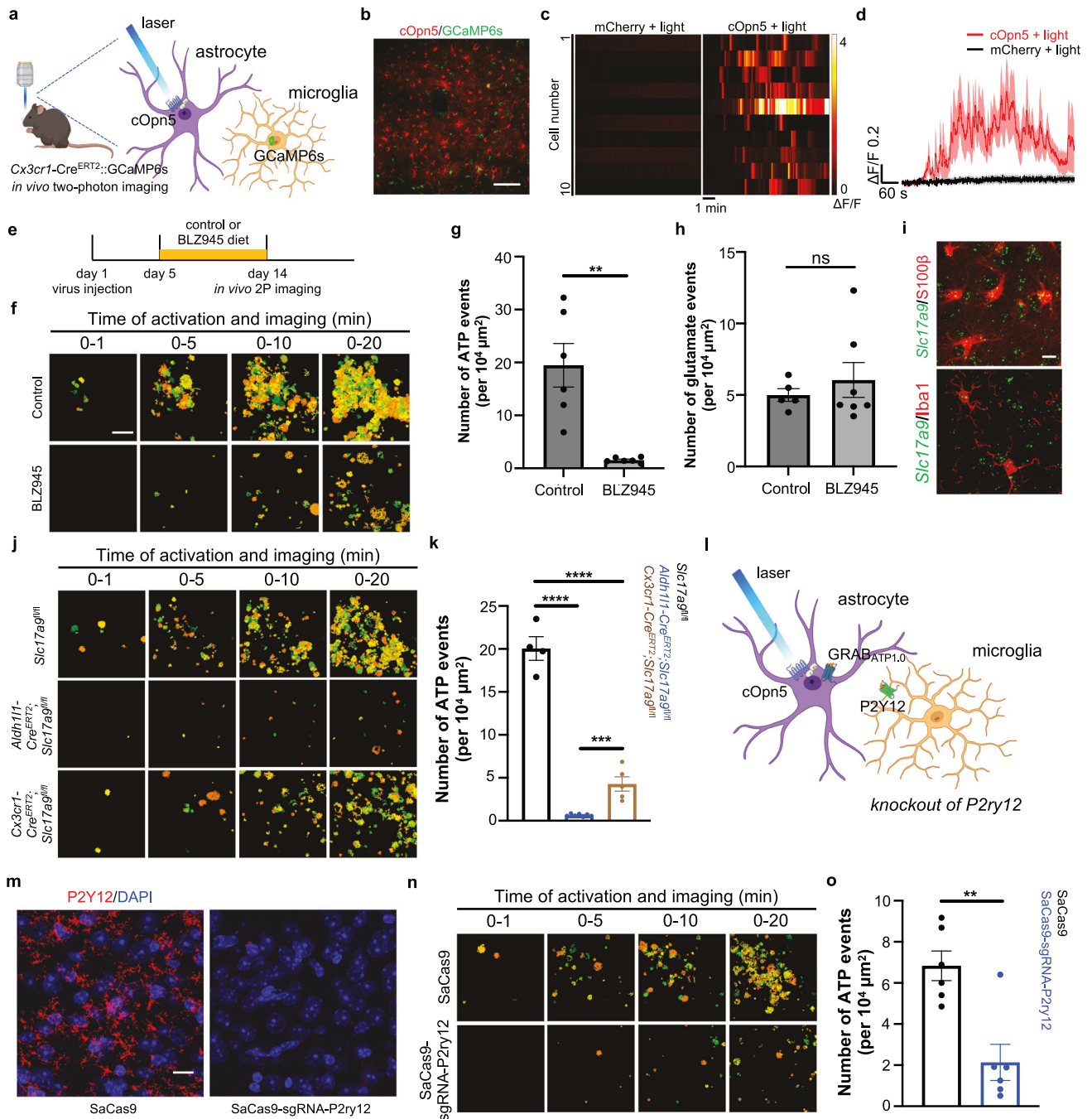
Fig. 4 Microglia amplify extracellular ATP/ADP signals by astrocytes. a Diagrams outlining the experimental design to investigate the impact of optogenetic astrocyte activation on Ca²⁺ signaling in microglia. We expressed GCaMP6s in microglia through mouse cross-breeding and cOpn5 in astrocytes using AAV vectors. **b** Two-photon microscopy images exemplifying bicistronic expression of cOpn5 and mCherry within astrocytes and separate GCaMP6s expression in microglia. Scale bar, 100 μm. **c** Heatmap representation of Ca²⁺ signals within individual microglia in which astrocytes expressed either mCherry alone (left) or cOpn5 (right) ($n = 10$ cells per group). **d** Time-course traces of GCaMP fluorescence changes in microglial populations from mice expressing cOpn5 in astrocytes compared to those expressing mCherry alone ($n = 10$ cells per group). **e** Schematics of the experimental procedure for microglial depletion. BLZ945 treatment was initiated 4 days post-virus injection surgery. Acute craniotomy and two-photon imaging were performed 9 days later. Representative images (**f**) and group data (**g**) showing ATP/ADP-release events in control or BLZ945-treated mice ($n = 6$ mice per group). **h** Group data showing the number of glutamate release events during 10 min in the control diet-fed or BLZ945-treated mice ($n = 6$ mice per group). Unpaired t-tests. **i** Confocal images displaying fluorescent in situ hybridization (FISH) signals of *Slc17a9* and immunohistochemical (IHC) staining for S100β or Iba1 markers. Scale bar, 10 μm. Representative images (**j**) and comparative group data (**k**) illustrating ATP/ADP-release events in *Slc17a9*^fl/fl control mice ($n = 4$ mice), *Aldh1l1*-Cre^ERT2^::*Slc17a9*^fl/fl mice ($n = 7$ mice), and *Cx3cr1*-Cre^ERT2^::*Slc17a9*^fl/fl mice ($n = 5$ mice). **l** Schematic representation of the experimental strategy for *P2ry12* knockout using AAV vectors and its effect on ATP/ADP release upon astrocyte activation. **m** Confocal images of P2Y12 IHC signals in mouse brain sections, demonstrating the efficiency of the knockout. Scale bar, 10 μm. Representative images (**n**) and group data (**o**) comparing ATP/ADP-release events in *P2ry12* knockout (SaCas9-sgRNA-P2ry12) and control (SaCas9) mice ($n = 6$ mice per group). Error bars in **g**, **h**, **k**, and **o** indicate SEM. ns, $p > 0.05$; **$p < 0.01$; ****$p < 0.0001$; unpaired t-tests. See Supplementary Table S1 for detailed information about inferential statistical tests.

including both ionotropic (P2X4, P2X7) and metabotropic (P2Y1, P2Y2, P2Y12) types, which are involved in modulating microglial activation, mobility, and signaling [60–62]. Of particular interest is P2Y12, primarily expressed in microglia and playing a vital role in early-stage microglial activation mediated by ATP/ADP [63]. To test its role, we employed AAV-MG1.2, an AAV variant efficient for in vivo microglial transduction [64], to deliver SaCas9 and sgRNA targeting *P2ry12* while expressing cOpn5 and GRAB$_{ATP1.0}$ in the astrocytes (Fig. 4l, m). Imaging results demonstrated a significant decrease in ATP/ADP release post-astrocytic activation from *P2ry12* knockout (Fig. 4n, o).

These findings indicate that microglia, upon sensing ATP/ADP released by astrocytes through P2Y12, further engage in VNUT-dependent exocytosis to release ATP/ADP themselves, which accounts for the massive ATP/ADP release upon cOpn5-mediated activation of astrocytes. This underscores a previously unrecognized cooperative mechanism between astrocytes and microglia in the gliotransmission of ATP/ADP.

LPS induces VNUT-dependent ATP/ADP release from astrocytes and microglia

To examine whether astrocytes and microglia contribute to ATP/ADP release via vesicular exocytosis in a physiological context, we focused on inflammation stress, a scenario relevant for both cell types [65, 66]. Given that lipopolysaccharide (LPS), a potent pro-inflammatory agent from Gram-negative bacteria elicits robust inflammatory responses in the brain [67], we established an inflammation model by administering a single intraperitoneal dose of 20 mg/kg LPS to mice (Fig. 5a). Eight hours post-LPS injection, we observed significantly elevated CD68 and GFAP expression, markers of microglial and astrocyte activation, respectively (Fig. 5b, c), confirming their inflammatory response.

GRAB$_{ATP1.0}$ imaging from cortical astrocytes revealed infrequent ATP/ADP release events at baseline levels, approximately 0.4 per 10^4 µm² during 20 min in awake mice (Fig. 5d, g). The number of ATP/ADP release events gradually increased at 2, 4, and 6 hours after LPS injection, reaching 3 per 10^4 µm² at 6 h (Fig. 5d, g). Analyzing the fluorescence dynamics of LPS-induced ATP/ADP release revealed that the fluorescent flashes varied in size from one hundred to thousands of square micrometers (median 206 µm², 1st quartile 103 µm², 3rd quartile 408 µm²) and in duration from a few seconds to over one hundred seconds (median 21 s, 1st quartile 11 s, 3rd quartile 42 s) (Fig. 5e, f), exhibiting slightly different characteristics from ATP/ADP release induced by cOpn5-mediated optogenetic activation of astrocytes, with a smaller area and shorter duration (Fig. 1m, n). These differences might arise from the distinct contributions of astrocytes and microglia to ATP/ADP release under LPS-induced brain inflammation and cOpn5-mediated optogenetic activation of astrocytes.

Knockout of *Slc17a9* did not alter baseline levels but significantly inhibited LPS-induced ATP/ADP release at 6 h (Fig. 5d, g), demonstrating VNUT dependence. We noted that LPS-induced ATP/ADP release was not completely blocked by the knockout of *Slc17a9*, with a value of 0.8 per 10^4 µm² at 6 h (Fig. 5d, g), suggesting a VNUT-independent component of gliotransmission in brain inflammation. Conditional knockout of *Slc17a9* in astrocytes or microglia partially replicated the effects of general knockout, indicating that both types of glial cells contributed to ATP/ADP release in a VNUT-dependent manner in LPS-induced brain inflammation (Fig. 5d, g).

DISCUSSION

Astrocytes, once considered mere support structures, are now recognized for releasing gliotransmitters that modulate neuronal activity, cerebral blood flow, and various mental processes [21, 25, 68–71]. However, the in vivo dynamics of gliotransmitter release remain poorly understood due to technical limitations in astrocyte activation and gliotransmitter monitoring. Here, we utilized the optogenetic tool cOpn5 to induce Ca²⁺ signals in astrocytes and employed two-photon imaging to visualize the release of the most studied gliotransmitters, ATP/ADP, and glutamate, using genetically encoded fluorescent sensors. We discovered that extended astrocyte activation produces flash-like release events, characterized by spatiotemporal dynamics markedly different from conventional neurotransmitter release. Both ATP/ADP and glutamate releases were identified as Ca²⁺-dependent vesicular exocytosis. Moreover, ATP/ADP release involves a VNUT-dependent signaling pathway and recruits microglia activity during optogenetic activation of astrocytes and LPS-induced inflammatory stress. These findings have several implications for understanding the mechanisms and functions of gliotransmission.

Gliotransmission of ATP/ADP and glutamate exhibit drastically different spatiotemporal features from those of neurotransmitter release, which is characterized by rapid onset (within milliseconds after an action potential), fast kinetics (lasting milliseconds within the synaptic cleft), and tight localization (submicron scale) [72]. In contrast, ATP/ADP and glutamate release begin approximately two minutes following stimulation onset, with peak release occurring around the 6–8 min mark. Individual flashes of ATP/ADP and glutamate persist for up to one minute and cover areas with diameters in the range of ~10 µm. These features challenge the conventional understanding of Ca²⁺-dependent vesicular release by neurons. Unlike neurons, astrocytes lack the specialized machinery for millisecond-scale rapid vesicle priming, fusion, and release typically seen in neurotransmission [2]. Instead, they contain various types of vesicular organelles, including dense-core vesicles, lysosomes, and exosomes, which differ from synaptic vesicles in size, origin, cargo, membrane composition, dynamics, and functions [3, 73]. Prior in vitro and ex vivo studies have proposed that regulated ATP/ADP release from astrocytes might occur through mechanisms like lysosome exocytosis, which depends on the accumulation of Ca²⁺-induced downstream processes or the maintenance of Ca²⁺ oscillations [13, 74]. The timing of ATP/ADP and glutamate release we observed aligns with the delayed onset of lysosomal exocytosis reported in the literature [75], hinting that gliotransmitter release is mediated by a distinct vesicular pathway rather than traditional synaptic vesicle exocytosis.

Our data suggest that vesicular exocytosis of gliotransmitters might be rare events, requiring strong and prolonged Ca²⁺ signals within astrocytes. However, once triggered, each release event has the potential to impact receptor activity over extensive neural territories. Vesicular organelles in astrocytes, especially those originating from lysosomes [13], can measure over 1000 nm in diameter [76], whereas synaptic vesicles have a more uniform size around 40 nm [77]. Consequently, individual astrocytic vesicles may encapsulate substantially larger quantities of transmitter molecules than synaptic vesicles, producing large and prolonged flashes. Their effects could be further modulated by extracellular metabolism, diffusion, and reuptake mechanisms. We show that astrocyte-derived ATP/ADP undergoes enzymatic conversion to adenosine via the ectonucleotidase CD73, potentially broadening the astrocytic influence to a more extensive array of cells or synapses post-ATP/ADP release and subsequent hydrolysis.

Our observations of extensive ATP/ADP and glutamate releases imply that gliotransmission could be a general ability of astrocytes. Two-photon imaging, with its optical sectioning thickness of a few micrometers, likely limits activation and imaging to around 100 astrocytes within the imaging areas. We recorded over 500 ATP/ADP and approximately 200 glutamate flashes in this area within the first 10 min, suggesting that the majority of astrocytes might release ATP/ADP and glutamate upon strong activation. The notable frequency of glutamate release is particularly significant, considering previous research
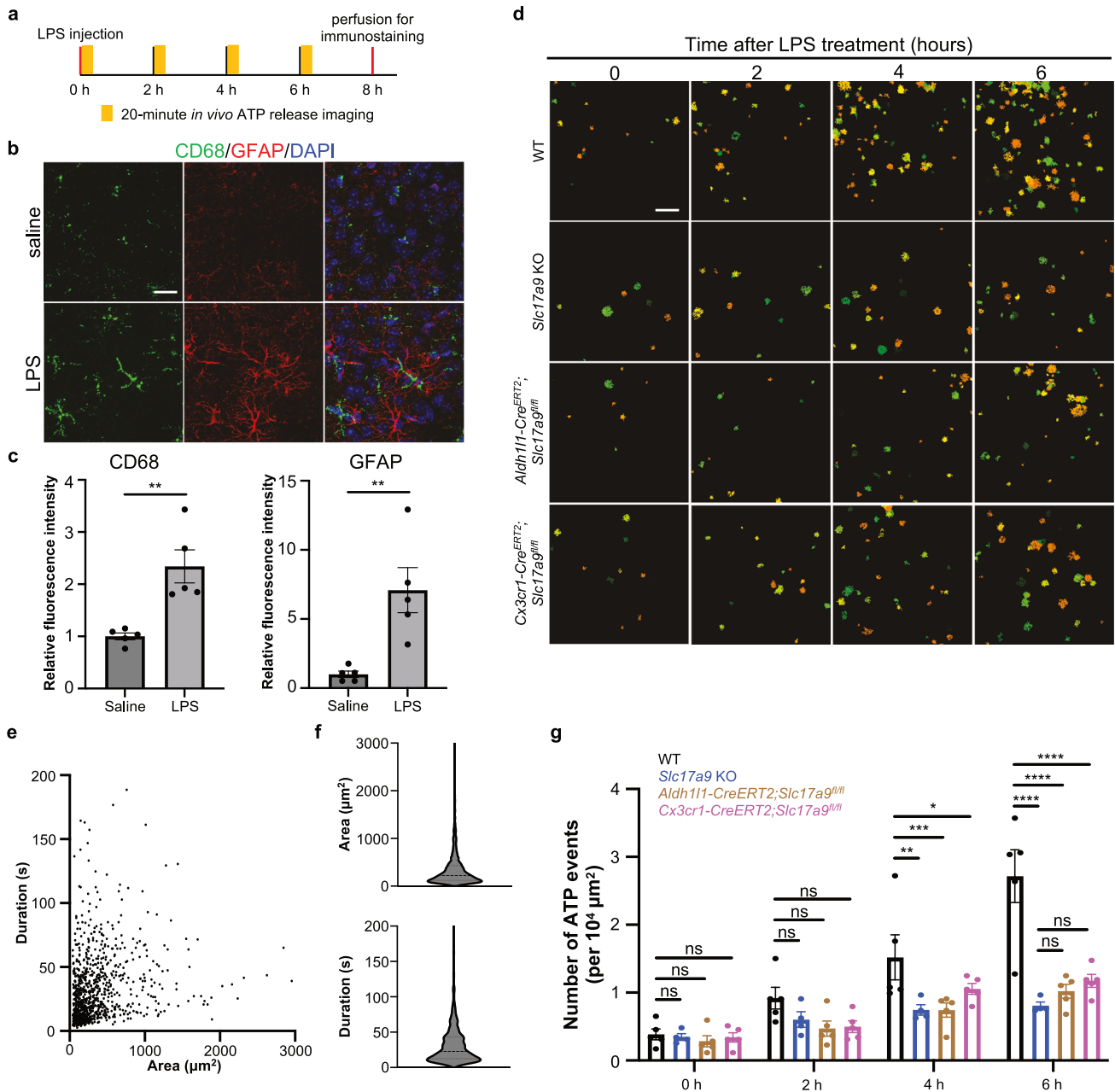
Fig. 5 VNUT in astrocytes and microglia contributes to LPS-induced ATP/ADP release. a Diagrammatic overview of the experimental protocol. Twenty-minute imaging sessions were conducted at baseline (0 h) and 2, 4, and 6 h post-single LPS injection (20 mg/kg, i.p.). Mice were perfused for IHC staining 8 h subsequent to LPS administration. **b** Confocal images depicting CD68 and GFAP IHC signals, showcasing microglial and astrocytic activation 8 hours post-LPS treatment. Optical Z-stack thickness, 30 μm. Scale bar, 20 μm. **c** Quantitative analysis of IHC signals for CD68 and GFAP, normalized relative to the saline control group ($n = 5$ imaging areas from 2 mice each). Unpaired t-tests. **d** Representative images of ATP/ADP-release events captured within 20-minute sessions, at 0, 2, 4, and 6 h post-LPS administration in wild-type (WT) mouse, *Slc17a9* whole-knockout, and respective *Slc17a9* conditional knockout mice targeting astrocytes and microglia. Scale bar, 100 μm. Scatter plots (**e**) and violin plots (**f**) illustrating the distribution of area and duration of individual ATP/ADP release events induced by LPS treatment ($n = 977$ events). Horizontal dashed lines in **f** indicate the first quartile, median, and third quartile. **g** Comparative group data of ATP/ADP-release events within 20 min, imaged at 0, 2, 4, and 6 h post-LPS treatment ($n = 5$ mice in WT group, 4 mice in *Slc17a9* KO group, 5 mice in *Aldh1l1*-Cre^{ERT2}::*Slc17a9*$^{fl/fl}$ group, and 5 mice in *Cx3cr1*-Cre^{ERT2}::*Slc17a9*$^{fl/fl}$ group). Two-way ANOVA. Error bars in **c** and **g** indicate SEM. ns, $p > 0.05$; *$p < 0.05$; **$p < 0.01$; ***$p < 0.001$; ****$p < 0.0001$. See Supplementary Table S1 for detailed information about inferential statistical tests.

showing that astrocytes abundantly express glutamine synthetase, which converts glutamate to glutamine and thus potentially restricts intracellular glutamate levels from reaching the threshold necessary for release [78].

Our findings offer new insights into the debate on gliotransmitter release mechanisms. In cultured cells and acute brain slices, ATP/ADP can be released through both Ca^{2+}-dependent vesicular exocytosis and the opening of membrane channels, particularly under pathological conditions like neuronal injury and tissue damage [23, 25, 79–81]. Cultured astrocytes can also release glutamate through channels [24], although this mechanism remains to be confirmed in vivo. The dependence on *Itpr2*

and SNARE in some studies suggested ATP/ADP release via vesicular exocytosis in vivo, but direct visualization has been limited [69]. Here, ATP/ADP and glutamate releases are inhibited by both Gq inhibitors and Ca^{2+} chelators, indicating Ca^{2+} dependence. V-ATPase inhibitors, which disrupt proton pumping and vesicle acidification, and TeNT expression, which blocks vesicle SNARE machinery, also significantly reduced the releases, suggesting the necessity of vesicular packaging and fusion.

Most importantly, *Slc17a9/VNUT* knockout in astrocytes markedly diminishes ATP/ADP flashes, reinforcing the role of a vesicular release mechanism. Despite low VNUT expression in astrocytes [82], it has been associated with ATP/ADP storage in secretory lysosomes [50] and the ATP/ADP release [19, 83–85]. Collectively, these prior findings, along with our current research, indicate that even low VNUT levels are crucial for ATP/ADP release from astrocytes. The specific vesicular glutamate transporter in astrocytes remains unidentified, though the limited expression of the solute carrier (SLC) group of membrane transport proteins vGlut1-3 is noted [2, 86]. A small subpopulation of astrocytes uses vGlut1 to concentrate glutamate into vesicles and release it rapidly in a pattern similar to neuronal glutamate release [27]. Our findings of large and prolonged glutamate flashes suggest an additional form and mechanism of glutamate release by some astrocytes, potentially involving an undiscovered vesicular glutamate transporter. This could be identified through a combination of optogenetic stimulation of astrocytes, glutamate imaging, and comprehensive knockout of genes encoding the SLC transporters. Collectively, our data strongly support Ca^{2+}-dependent vesicular exocytosis for ATP/ADP and glutamate, offering new avenues for identifying astrocyte-specific vesicular glutamate transporters.

Interestingly, astrocytes interact with microglia during ATP/ADP release but not glutamate release. Optogenetic activation of astrocyte Gq signaling induces a rapid elevation in microglial Ca^{2+} signals and morphological changes. Depleting microglia or knocking out microglial *Slc17a9* or *P2ry12* significantly reduces, but does not eliminate, ATP/ADP flashes in response to astrocyte activation while not affecting glutamate release. We propose that activated astrocytes release ATP/ADP in flashes, activating microglial P2Y12, increasing Ca^{2+} signals [87], and leading to microglial ATP/ADP release in a VNUT-dependent manner. On the other hand, our results suggest that microglia do not release glutamate following ATP/ADP detection and that ATP/ADP from microglia does not influence astrocytic glutamate release.

Our findings unveiled that under conditions of LPS-induced brain inflammation, both astrocytes and microglia become activated and release ATP/ADP in a VNUT-dependent manner. This underscores that vesicular exocytosis of ATP/ADP is not merely an artifact of intense optogenetic stimulation but holds relevance in certain physiological and pathological contexts. Prior research has highlighted cytokine-mediated interactions between glial cells in the etiology and progression of neurological disorders, such as multiple sclerosis [88], inflammation [89], and other neuropathies [14, 89, 90]. Our results suggest that vesicular ATP/ADP release constitutes an additional mechanism that orchestrates the bidirectional communication between astrocytes and microglia, thereby modulating glial cell interactions in health and disease. Exploring the astrocytic release of ATP/ADP and glutamate across diverse behavioral states in the future will be instrumental in elucidating the full spectrum of physiological functions attributed to astrocytic gliotransmission.

Our experimental approaches also establish a paradigm for studying gliotransmitter release and glial functions. cOpn5-mediated optogenetics outperforms channel-based tools like ChR2 by more effectively generating strong Ca^{2+} dynamics in astrocytes [17, 70] and triggering significant releases of ATP/ADP and glutamate. Optogenetic stimulation via the Gi-coupled eOpn3 produces transient Ca^{2+} signals in astrocytes, triggering gliotransmitter release with less efficiency than cOpn5 optogenetics. In contrast, Gq-based chemogenetic activation produces prolonged yet static Ca^{2+} increase primarily in the soma region and is far less efficient at inducing gliotransmitter release. These findings underscore the importance of spatiotemporally dynamic Ca^{2+} signals, irrespective of specific G-protein signaling pathways, in mediating gliotransmitter release. Optogenetic methods, unlike mechanical, electrical, or pharmacological approaches, allow for cell-type specificity in vivo. Combining genetically encoded gliotransmitter sensors $GRAB_{ATP1.0}$ and iGluSnFR with two-photon imaging enables precise spatiotemporal mapping of release patterns over a large field, revealing distinct characteristics of ATP/ADP and glutamate flashes not captured by traditional methods such as the "sniffer-patch" technique and microdialysis [24, 69]. These strategies could be applied to study other gliotransmitters with available sensors, like GABA and neuropeptide Y [91–93], and potentially for additional ones like D-serine and taurine, upon the development of suitable fluorescent sensors.

METHODS
All methods were performed following the relevant guidelines and regulations.

Experimental models
Animal care and use strictly followed the approval of the Animal Care and Use Committee of the National Institute of Biological Sciences, Beijing (Approval ID: NIBS2022M0036) and the Chinese Institute for Brain Research, Beijing (Approval ID: CIBR-IACUC-001), following the Regulations for the Administration of Affairs Concerning Experimental Animals of China.

We obtained *Cx3cr1*-CreERT2 mice (JAX strain 021160), Cx3cr1-GFP mice (JAX Strain 005582), and GCaMP6 mice (JAX Strain 024106) from Jackson Laboratory. We purchased *Slc17a9* KO mice from Cyagen Biosciences (Serial Number: KOCMP-03312-Slc17a9). *CD73* KO mice were kindly provided by Dr. Jiangfan Chen (Wenzhou Medical University) and *Aldh1l1*-CreERT2 mice were gifts from Dr. Tianming Gao (Southern Medical University). The *Slc17a9*fl/fl transgenic mice (Clone No., EPD0424_2_F09) were generated by CAM-SU Genomic Resource Center and were kindly provided by Dr. Yulong Li (Peking University). Adult C57BL/6J wildtype mice were obtained from Beijing Vital River Laboratory Animal Technology and Laboratory Animal Resource Center, Chinese Institute of Brain Research, Beijing. We used mice aged 7-10 weeks for our experiments and male or female mice were randomly used. Mice were housed in groups of no more than five under a reverse 12/12 light/dark cycle, with ad libitum access to food and water. All experiments were conducted during the dark phase.

Viral vectors
AAV vectors, including AAV2/8-GfaABC1D-cOpsin5-T2A-mCherry-WPRE-pA, AAV2/8-GfaABC1D-TeNT (LC)-mCherry, AAV2/8-GfaABC1D-TeNT (LC, E234A)-mCherry, AAV-MG1.2-CMV-SaCas9-U6-sgRNA-P2ry12, and AAV-MG1.2-CMV-SaCas9 were packaged with titers ranging from 5 to 15 $\times 10^{12}$ viral genomes (v. g.)/mL following established protocols from Minmin Luo's Lab [94]. The production process entailed co-transfecting the respective AAV vectors and the AAV helper plasmids into HEK 293T cells. Cells were harvested 96 h after transfection, and the viral particles were released from cells by freeze-thaw cycles and sonication. Subsequently, purification was accomplished via cesium chloride density gradient ultracentrifugation, with the final product being dialyzed into phosphate-buffered saline (PBS) buffer. Titration of the AAV vectors was achieved using quantitative polymerase chain reaction (qPCR). Other AAV vectors utilized in the study, namely AAV2/8-GfaABC1D-mCherry-WPRE-pA, AAV2/8-GfaABC1D-GCaMP6s-WPRE-pA, AAV2/9-hsyn-mCherry-P2A-TetTox-WPRE-pA, AAV2/9-mCaMK2a-jGCaMP7b-WPRE-pA, and AAV2/9-hsyn-SF-iGluSnFR(A184S)-WPRE-pA were purchased from Shanghai Taitool Bioscience Co., China. AAV2/8-GfaABC1D-GRAB$_{ATP1.0}$-WPRE-pA was purchased from Vigene Biosciences, China. AAV2/9-hsyn-iGluSnFR3.v857.GPI was purchased from Braincase, China. AAV2/5-hsyn-iATP/ADPSnFR1.0-WPRE-hGH-polyA was purchased from BrainVTA, China. AAV2/9-hsyn-GRAB$_{Ado1.0m}$-WPRE-pA was kindly provided by Dr. Yulong Li (Peking University).

HEK 293T cell culture and Ca²⁺ imaging

Human Embryonic Kidney (HEK) 293T cells were obtained from the American Type Culture Collection (ATCC) and were maintained under standard conditions at 37 °C in a humidified atmosphere containing 5% carbon dioxide. The culture medium consisted of Dulbecco's Modified Eagle Medium (DMEM) enriched with 10% (volume per volume) fetal bovine serum (FBS) and 1% penicillin-streptomycin solution. For establishing cOpn5-expressing stable cell lines, cell-filling version of chicken Opn5 was constructed using a ribosomal skip site (T2A) between the opsin and fluorescent proteins, which was then subcloned into a lentiviral backbone pLJM1 vector (Addgene plasmid #19319) under a CMV promoter to make vector pLJM1-cOpn5-T2A-EGFP. Lentivirus was packaged using the pLJM1-cOpn5 vector and was then used to transduce HEK 293T cells. After transduction, positive cells were selected by treating them with 5 µg/ml puromycin. Continuous antibiotic pressure was enforced to uphold prolonged gene expression.

Before calcium imaging, HEK 293T cells were loaded with Ca²⁺ indicator Calbryte 630-AM at a concentration of 5 µM in Hank's Balanced Salt Solution (HBSS) buffer for an hour. Upon completion of dye incubation, the solution was replaced with 2 mL of HBSS to wash out excess dye, and measures were taken to shield cells from ambient light exposure to avoid unintended activation during the incubation period preceding imaging. For mapping the two-photon excitation spectrum of cOpn5, STELLARIS 8 DIVE Multiphoton Microscope (Leica Microsystems, equipped with a 25× water immersion objective lens, numerical aperture 1.05) was employed. Fluorescence Recovery After Photobleaching (FRAP) mode was applied, utilizing a 633 nm one-photon laser for calcium imaging, while a tunable 800/850/920/960/1000/1045 nm two-photon laser was sequentially used to stimulate cOpn5 in predefined regions of interest (ROIs). Imaging and optogenetic stimulation occurred at a rate of 1.5 frames per second (fps), with each experimental run comprising an initial capture of 20 baseline frames, followed by a 3-frame optogenetic stimulus, and concluded with 100 frames to document alterations in intracellular calcium levels. The intensity of the optogenetic activation laser was consistently regulated across experiments involving different two-photon wavelengths and was set below the levels typically employed in in vivo two-photon imaging experiments, i.e., no higher than 12 mW.

Single molecule fluorescent in situ hybridization histochemistry

For single molecule fluorescent in situ hybridization (smFISH) combined with immunohistochemistry, mice were initially perfused with 1X phosphate-buffered saline (PBS) and subsequently fixed using 4% paraformaldehyde (PFA) in PBS. Their brains were then immersed in 4% PFA overnight, followed by a dehydration stage in 30% sucrose solution. Brain tissues were sliced into 20 micrometer-thick sections utilizing a Leica CM1950 cryostat microtome. Pretreatment of these sections adhered to the User Manual of ACDBio RNAscope Multiplex Fluorescent Regent Kit v2 (ACDBio #323100) and RNA-Protein Co-Detection Ancillary Kit (ACDBio #323180). In summary, following initial air-drying at −20 °C for two hours and baking at 60°C for half an hour, fixed frozen tissue sections were subjected to an additional 15-min postfixation in 4% PFA under four °C, and sequentially dehydrated through a range of concentration of EtOH. They were next processed with hydrogen peroxide to quench endogenous peroxidases and underwent target retrieval procedures. Thereafter, sections were incubated overnight at four °C with primary antibodies against S100β or Iba1, diluted at 1:200. After that, samples were treated with hydrogen peroxide and target retrieval steps before incubation with primary antibodies (anti-S100β or anti-Iba1, 1:200) at four °C overnight. Following primary antibody incubation, samples were treated with post-primary fixation and protease steps. Then, samples were incubated with the RNAscope probe for 2 h at 4 °C. A custom-made RNAscope probe to specifically detect Slc17a9 was purchased from ACDBio (Mm-Slc17a9, #873591, target region: 385-1301 base pairs). This was followed by a tripartite amplification sequence, with visualization achieved using TSA Vivid 520 dye (1:1000 dilution). Subsequently, sections were incubated with Alexa Fluor 647 AffiniPure Goat Anti-Rabbit IgG secondary antibody (1:200 dilution) for 30 min at room temperature. Counterstaining with DAPI and coverslipping with Prolong Gold antifade mountant finalized the sample preparation.

Specifically, layer 2/3 of the S1 cortex was imaged under a Leica SP8 confocal laser scanning microscope, employing a 40x oil immersion objective lens (NA 1.3), 3x digital zoom, a pixel resolution of 1024 × 1024, and a z-step of 0.35 micrometers to generate confocal stacks spanning approximately 10 to 15 micrometers. Throughout each experiment, laser parameters were consistently maintained to ensure comparability of imaging results.

Single-cell suspension preparation and Flow cytometry

C56BL/6J, Slc17a9 KO, Slc17a9^fl/fl, Aldh1l1-Cre^ERT2;Slc17a9^fl/fl, and Cx3cr1-Cre^ERT2;Slc17a9^fl/fl mice were anesthetized with avertin and cardiac perfusion was performed with ice-cold saline. The cranial region was sanitized with ethanol, the scalp carefully dissected away, and the skull gently removed using surgical scissors and forceps to expose the brain. The extracted brain was promptly immersed in ice-chilled Dulbecco's Phosphate-Buffered Saline (DPBS) for an initial rinse. Subsequently, the brain was relocated to a 6-well plate filled with 2 mL of digestion mixture composed of Dulbecco's Modified Eagle Medium (DMEM), 16 Units per milliliter of papain, and 40 Units per milliliter of DNase. It was then diced into minute fragments. This mixture was shifted to a 15 mL tube and maintained at 37 °C for half an hour, with intermittent gentle swirling every five minutes. Post-incubation, 3 mL of complete DMEM was introduced to halt enzymatic activity. The contents were gently mixed until all visible aggregates dispersed, passing the suspension through successive 70 µm and 40 µm cell strainers to isolate single cells. The filtrate was gathered into a fresh 15 mL tube, centrifuged at 1600 rpm for ten minutes, the supernatant discarded, and the cell pellet resuspended in 1 mL of ice-cold DPBS. For immunophenotyping, microglia were labeled with CD11b-PE, while astrocytes were marked with ACSA2-APC. Antibodies were added to the single-cell suspension and incubated for 30 min on ice in the dark. Following incubation, the suspension was spun down at 1000 rpm for three minutes, rinsed once more with ice-cold DPBS under the same centrifugation conditions, and the pellet was resuspended in 2 mL of ice-cold DPBS. Finally, the cell suspension was subjected to analysis and sorting using the advanced BD FACSAria III flow cytometer.

RNA isolation and quantitative PCR

In the process of conducting whole-brain and single-cell Reverse Transcription-Polymerase Chain Reaction (RT-PCR), RNA extraction was meticulously executed adhering to the protocol provided by the FastPure Cell/Tissue Total RNA Isolation Kit V2, sourced from Vazymes (Catalog Number RC112-01). The synthesis of complementary DNA (cDNA) was accomplished by complying with the guidelines of TransScript One-Step gDNA Removal and cDNA Synthesis SuperMix, a product of TransGen Biotechs (Catalog Number AT311-02). Quantitative real-time PCR (qPCR) was carried out following the instructions detailed in the PerfectStart Green qPCR SuperMix manual, also from TransGen Biotechs (Catalog Number AQ601-01-V2), utilizing a Rocgene Archimed X qPCR system.

The cycling conditions entailed an initial denaturation step at 95 °C for 10 min, succeeded by 45 cycles of amplification, each consisting of 95 °C for 15 s, 60 °C for 60 seconds, and concluded with a final extension at 25 °C for 15 s.

The relative quantification of SLC17A9 mRNA expression was assessed through the comparative Ct (cycle threshold) method, yielding the ratio of SLC17A9 to the internal control GAPDH. Gene expression levels were further analyzed using the 2^-ΔΔCt formula. All primer sequences were meticulously designed utilizing the NCBI Primer-BLAST tool to ensure specificity and efficiency.

GAPDH Forward Primer: AGGTCGGTGTGAACGGATTTG
GAPDH Reverse Primer: TGTAGACCATGTAGTTGAGGTCA
SLC17A9 Forward Primer: CAGGAGAGCGAGAGAGCCTT
SLC17A9 Reverse Primer: TGAGGCCACCTGAGAAGTAGA

Tamoxifen administration

Tamoxifen was dissolved in corn oil to a concentration of 10 mg/kg under continuous stirring at 37 °C, and subsequently stored at 4 °C for a duration of 5 days to ensure proper formulation. To attain microglia-specific expression of GCaMP6s in Cx3cr1-Cre^ERT2::GCaMP6s mice, microglia-specific knockout of Slc17a9 in Cx3cr1-Cre^ERT2::Slc17a9^fl/fl mice, and astrocyte-specific knockout of Slc17a9 in Aldh1l1-Cre^ERT2::Slc17a9^fl/fl mice respectively, adult animals underwent a regimen of daily intraperitoneal tamoxifen injections at a dosage of 100 mg per kg of body mass for a consecutive period of 5 days. Mice serving as controls (Slc17a9fl/fl) also underwent this tamoxifen administration schedule to maintain parity. Experimental procedures were initiated four weeks post the conclusion of tamoxifen induction to allow for adequate genetic modification manifestation.

Intracranial injections and open-skull surgery

Mice were anesthetized with avertin (i.p., 250 mg/kg) and mounted to a stereotaxic apparatus (RWD Co., China). A small craniotomy was performed above the primary somatosensory (S1) cortex. Adeno-associated viral (AAV) vectors were infused transcranially through this opening utilizing a Micro4 controller paired with a microsyringe pump (Nanoliter 2010 Injector from WPI). Stereotaxic coordinates aimed at the S1 cortex were precisely (−1.58 mm anterior-posterior, ±2.25 mm medial-lateral, −1.25 mm dorsal-ventral) from the bregma reference point. Infusions occurred at a pace of 60 nL/min, with a total infusion volume of either 900 nL for single AAV vectors or 1200 nL when combining two or three vectors. In experiments necessitating co-expression of multiple viral vectors, equal titer vectors were thoroughly blended in a 1:1 volumetric ratio prior to injection. Post-injection, the craniotomy site was sealed with bone wax to inhibit connective tissue overgrowth, and the incision on the scalp was sutured shut. Fourteen days was allowed for virus expression post-procedure. Thereafter, mice were again anesthetized, and a 3 mm diameter skull aperture was drilled at the viral injection location, which was then overlaid by a glass window. A stainless-steel head-restraining bar, integrated with an imaging chamber, was then placed atop the window and affixed firmly with dental cement. In cOpn5 optogenetic experiments, acute skull preparations were executed immediately before imaging sessions, and illuminated areas were cautiously shielded post-craniotomy to prevent unintended light exposure. Mice were maintained under avertin-induced anesthesia during imaging sessions. For the intracerebral application of drugs, the solution diluted to 1 mM concentration in PBS was delivered using a Micro4 controller and micro syringe pump at a rate of 60 nL/min with a total volume of 1 μL before covering a glass window.

In chemogenetic and LPS treatment experiments, mice were allowed to recover for one week after open-skull surgery before imaging and remained awake during imaging.

In vivo two-photon imaging

As mentioned in the open-skull surgery section, in cOpn5 optogenetic experiments, the mice with acute skull window were under anesthesia and held in place by customized head-fixing bars during two-photon imaging. Images were acquired 100–150 μm below the dura mater using a STELLARIS 8 DIVE Multiphoton Microscope (Leica, 25× water-immersion lens with NA 1.05). To stimulate cOpn5 and visualize fluorescence indicators concurrently, the laser was tuned to 920 nm with an intensity kept below 25 mW. For capturing mCherry signals, the laser was adjusted to 1045 nm at a similar intensity threshold. For simultaneous monitoring GCaMP, $GRAB_{ATP1.0}$, $GRAB_{Ado1.0m}$, or iGluSnFR fluorescence signal changes alongside cOpn5 activation, a 591.63×591.63 μm^2 field of view (512×512-pixel resolution) was imaged at 1.5 frames per second (fps.). To ensure that astrocytes were activated and the released gliotransmitter was detected, the fluorescence signals of cOpn5-T2A-mCherry and the sensors in the selected FOV should be strong enough at the same time. To avoid premature activation of cOpn5, the real-time imaging mode was switched off for 10 min after determining the imaging field of view. Then a time-lapse imaging session (xyt) was performed. The real-time imaging mode also needed to be switched off for 10 min when switching to another field of view.

In the LPS treatment and chemogenetic experiments, the mice remained awake. A 20-min baseline was acquired before the intraperitoneal injection of 20 mg/kg LPS. Imaging was then performed for 20 min at 0, 2, 4, and 6 h after LPS treatment to avoid attenuation of the sensor's fluorescence signal due to prolonged imaging. A 20-min baseline was also acquired before the intraperitoneal injection of 2 mg/kg CNO or an equivalent volume of saline and thereafter imaging was performed continuously for 60 min. Other imaging parameters were the same as for the cOpn5 optogenetic experiments.

To monitor spontaneous glutamate fluorescence transients using iGluSnFR3.v857.GPI, mice were allowed to recover for 1 week after open-skull surgery and remained awake during imaging. The laser was tuned to 1000 nm and its intensity was maintained below 30 mW for iGluSnFR3.v857.GPI imaging. A 295.18×295.18 μm^2 field of view (512×512-pixel resolution) was imaged at 2.5 frames per second (fps.).

Microglia depletion

Microglial ablation was accomplished through the administration of the Colony Stimulating Factor 1 Receptor (CSF1R) inhibitor, BLZ945 (Chem-Shuttle, Cat# 106245). For the purpose of microglial ablation in adult mice, a specialized diet was formulated incorporating BLZ945 at a concentration of 1200 mg per kg into an irradiation-sterilized, standard laboratory mouse breeding diet, supplied by Jiangsu Xietong Pharmaceutical Bio-engineering Co., Ltd. (Catalog Number 1010112). Adult mice undergoing this regimen of a BLZ945-supplemented diet for a continuous period of 9 days experienced comprehensive microglial clearance across the entire brain. To validate the efficacy of this depletion, immunohistochemical staining for the microglial-specific marker Iba1 was conducted following the completion of in vivo imaging experiments.

Immunohistochemistry

Mice were anesthetized with an overdose of pentobarbital and perfused intracardially with saline, followed by paraformaldehyde (PFA, 4% wt/vol in PBS). Brains were dissected and postfixed in 4% PFA for at least 4 h at room temperature. Samples were then dehydrated in a 30% sucrose solution. Brain sections (30 μm) were prepared on a Cryostat microtome (Leica CM1950). Sections were permeabilized with 0.3% Triton X-100 in PBS (PBST) and blocked in 3% BSA in PBST at room temperature for 1 h. Sections were then incubated with primary antibodies (anti-S100β, 1:1000, ab52642, Abcam; anti-NeuN, 1:1000, ab177487, Abcam; anti-Iba1, 1:1000, 019-19741, Wako; anti-P2RY12, 1:100, 848002, Biolegend) overnight at 4 °C. Samples were washed three times in PBS and were then incubated with fluorescent secondary antibodies (Goat anti-rabbit-AF647, 111-605-144, Jackson ImmunoResearch; Goat anti-rabbit-AF488, 111-545-003, Jackson ImmunoResearch; Goat anti-rat-Cy5, 112-175-143, Jackson ImmunoResearch) at room temperature for 2 hours. Samples were then washed three times in PBS. Fluorescent images were taken using a 40x (Oil, NA = 1.3, WD = 0.24 mm) objective lens, 1 digital zoom, 1024×1024 pixels, 0.35 μm step size to produce confocal stacks of ~20–30 μm on a confocal laser-scanning microscope (Leica SP8). Laser settings were kept the same within each experiment.

QUANTIFICATION AND STATISTICAL ANALYSIS

Lateral shifts in all two-photon images were corrected using ImageJ (FIJI) (Version 2.14.0) with the Image Stabilizer plug-in. We used the Astrocyte Quantitative Analysis (AQuA) program in MATLAB R2020a to quantify gliotransmitter fluorescence dynamics and numbers of release events, where the number of release events was normalized by the imaging area. In the AQuA program, the intensity threshold scaling factor, smoothing (sigma), and minimum size (pixels) were set to 2, 0.5, and 30 respectively to filter out background noise. Then we used customized MATLAB scripts to overlay images showing ATP/ADP or glutamate-release events identified by the AQuA program across time. For ROI-based time trace analysis of fluorescence signals, the Time Series Analyzer V3 plug-in in ImageJ was used. Then we used customized MATLAB scripts to calculate ΔF/F values and plot heatmap or time traces. Statistical significance was evaluated using Prism9 (Graph-Pad). Data were reported as means ± SEM in all figures. The exact P values and the corresponding inferential statistical methods are stated in figure captions and legends. Detailed information on statistical tests is provided in Supplementary Table S1.

DATA AVAILABILITY

All data necessary to assess the conclusions in this manuscript are provided in the main text or the supplemental information. Any additional information is available from the corresponding authors upon request.

CODE AVAILABILITY

All codes necessary to assess the conclusions in this manuscript are provided in the main text or the supplemental information. Any additional information is available from the corresponding authors upon request.

MATERIALS AVAILABILITY

All unique reagents generated in this study are available from the lead contact upon reasonable request.

REFERENCES

1. Khakh BS, Deneen B. The Emerging Nature of Astrocyte Diversity. Annu Rev Neurosci. 2019;42:187–207.
2. Chai H, Diaz-Castro B, Shigetomi E, Monte E, Octeau JC, Yu X, et al. Neural Circuit-Specialized Astrocytes: Transcriptomic, Proteomic, Morphological, and Functional Evidence. Neuron. 2017;95:531–49.e9.
3. Vardjan N, Parpura V, Verkhratsky A, Zorec R. Gliocrine System: Astroglia as Secretory Cells of the CNS. Adv Exp Med Biol. 2019;1175:93–115.
4. Parpura V, Zorec R. Gliotransmission: Exocytotic release from astrocytes. Brain Res Rev. 2010;63:83–92.
5. Harada K, Kamiya T, Tsuboi T. Gliotransmitter Release from Astrocytes: Functional, Developmental, and Pathological Implications in the Brain. Front Neurosci. 2015;9:499.
6. Shen W, Nikolic L, Meunier C, Pfrieger F, Audinat E. An autocrine purinergic signaling controls astrocyte-induced neuronal excitation. Sci Rep. 2017;7:11280.
7. Kofuji P, Araque A. Astrocytes and Behavior. Annu Rev Neurosci. 2021;44:49–67.
8. Chen J, Tan Z, Zeng L, Zhang X, He Y, Gao W, et al. Heterosynaptic long-term depression mediated by ATP released from astrocytes. Glia. 2013;61:178–91.
9. Brandebura AN, Paumier A, Onur TS, Allen NJ. Astrocyte contribution to dysfunction, risk and progression in neurodegenerative disorders. Nat Rev Neurosci. 2023;24:23–39.
10. McAlpine CS, Park J, Griciuc A, Kim E, Choi SH, Iwamoto Y, et al. Astrocytic interleukin-3 programs microglia and limits Alzheimer's disease. Nature. 2021;595:701–6.
11. Guthrie PB, Knappenberger J, Segal M, Bennett MV, Charles AC, Kater SB. ATP released from astrocytes mediates glial calcium waves. J Neurosci. 1999;19:520–8.
12. Duan S, Anderson CM, Keung EC, Chen Y, Chen Y, Swanson RA. P2X7 receptor-mediated release of excitatory amino acids from astrocytes. J Neurosci. 2003;23:1320–8.
13. Zhang Z, Chen G, Zhou W, Song A, Xu T, Luo Q, et al. Regulated ATP release from astrocytes through lysosome exocytosis. Nat Cell Biol. 2007;9:945–53.
14. Bezzi P, Domercq M, Brambilla L, Galli R, Schols D, De Clercq E, et al. CXCR4-activated astrocyte glutamate release via TNFalpha: amplification by microglia triggers neurotoxicity. Nat Neurosci. 2001;4:702–10.
15. Bazargani N, Attwell D. Astrocyte calcium signaling: the third wave. Nat Neurosci. 2016;19:182–9.
16. Tan Z, Liu Y, Xi W, Lou HF, Zhu L, Guo Z, et al. Glia-derived ATP inversely regulates excitability of pyramidal and CCK-positive neurons. Nat Commun. 2017;8:13772.
17. Li Y, Li L, Wu J, Zhu Z, Feng X, Qin L, et al. Activation of astrocytes in hippocampus decreases fear memory through adenosine A(1) receptors. Elife. 2020;9:e57155.
18. Figueiredo M, Lane S, Stout RF Jr, Liu B, Parpura V, Teschemacher AG, et al. Comparative analysis of optogenetic actuators in cultured astrocytes. Cell Calcium. 2014;56:208–14.
19. Lalo U, Palygin O, Rasooli-Nejad S, Andrew J, Haydon PG, Pankratov Y. Exocytosis of ATP from astrocytes modulates phasic and tonic inhibition in the neocortex. PLoS Biol. 2014;12:e1001747.
20. Martín R, Bajo-Grañeras R, Moratalla R, Perea G, Araque A. Circuit-specific signaling in astrocyte-neuron networks in basal ganglia pathways. Science. 2015;349:730–4.
21. Noh K, Cho WH, Lee BH, Kim DW, Kim YS, Park K, et al. Cortical astrocytes modulate dominance behavior in male mice by regulating synaptic excitatory and inhibitory balance. Nat Neurosci. 2023;26:1541–54.
22. Suadicani SO, Iglesias R, Wang J, Dahl G, Spray DC, Scemes E. ATP signaling is deficient in cultured Pannexin1-null mouse astrocytes. Glia. 2012;60:1106–16.
23. Chu J, Yang J, Zhou Y, Chen J, Chen KH, Zhang C, et al. ATP-releasing SWELL1 channel in spinal microglia contributes to neuropathic pain. Sci Adv. 2023;9:eade9931.
24. Woo DH, Han KS, Shim JW, Yoon BE, Kim E, Bae JY, et al. TREK-1 and Best1 channels mediate fast and slow glutamate release in astrocytes upon GPCR activation. Cell. 2012;151:25–40.
25. Yang J, Vitery MDC, Chen J, Osei-Owusu J, Chu J, Qiu Z. Glutamate-Releasing SWELL1 Channel in Astrocytes Modulates Synaptic Transmission and Promotes Brain Damage in Stroke. Neuron. 2019;102:813–27.e6.
26. Bezzi P, Gundersen V, Galbete JL, Seifert G, Steinhäuser C, Pilati E, et al. Astrocytes contain a vesicular compartment that is competent for regulated exocytosis of glutamate. Nat Neurosci. 2004;7:613–20.
27. de Ceglia R, Ledonne A, Litvin DG, Lind BL, Carriero G, Latagliata EC, et al. Specialized astrocytes mediate glutamatergic gliotransmission in the CNS. Nature. 2023;622:120–9.
28. Sloan SA, Barres BA. Looks can be deceiving: reconsidering the evidence for gliotransmission. Neuron. 2014;84:1112–5.
29. Savtchouk I, Volterra A. Gliotransmission: Beyond Black-and-White. J Neurosci. 2018;38:14–25.
30. Dai R, Yu T, Weng D, Li H, Cui Y, Wu Z, et al. A neuropsin-based optogenetic tool for precise control of G(q) signaling. Sci China Life Sci. 2022;65:1271–84.
31. Wu Z, He K, Chen Y, Li H, Pan S, Li B, et al. A sensitive GRAB sensor for detecting extracellular ATP in vitro and in vivo. Neuron. 2021;110:770–82.e5.
32. Marvin JS, Borghuis BG, Tian L, Cichon J, Harnett MT, Akerboom J, et al. An optimized fluorescent probe for visualizing glutamate neurotransmission. Nat Methods. 2013;10:162–70.
33. Marvin JS, Scholl B, Wilson DE, Podgorski K, Kazemipour A, Müller JA, et al. Stability, affinity, and chromatic variants of the glutamate sensor iGluSnFR. Nat Methods. 2018;15:936–9.
34. Adamsky A, Kol A, Kreisel T, Doron A, Ozeri-Engelhard N, Melcer T, et al. Astrocytic Activation Generates De Novo Neuronal Potentiation and Memory Enhancement. Cell. 2018;174:59–71.e14.
35. Vaidyanathan TV, Collard M, Yokoyama S, Reitman ME, Poskanzer KE. Cortical astrocytes independently regulate sleep depth and duration via separate GPCR pathways. Elife. 2021;10:e63329.
36. Nagai J, Rajbhandari AK, Gangwani MR, Hachisuka A, Coppola G, Masmanidis SC, et al. Hyperactivity with Disrupted Attention by Activation of an Astrocyte Synaptogenic Cue. Cell. 2019;177:1280–92.e20.
37. Mahn M, Saraf-Sinik I, Patil P, Pulin M, Bitton E, Karalis N, et al. Efficient optogenetic silencing of neurotransmitter release with a mosquito rhodopsin. Neuron. 2021;109:1621–35.e8.
38. Stachniak TJ, Ghosh A, Sternson SM. Chemogenetic synaptic silencing of neural circuits localizes a hypothalamus→midbrain pathway for feeding behavior. Neuron. 2014;82:797–808.
39. Gourine AV, Kasymov V, Marina N, Tang F, Figueiredo MF, Lane S, et al. Astrocytes control breathing through pH-dependent release of ATP. Science. 2010;329:571–5.
40. Lezmy J, Arancibia-Cárcamo IL, Quintela-López T, Sherman DL, Brophy PJ, Attwell D. Astrocyte Ca(2+)-evoked ATP release regulates myelinated axon excitability and conduction speed. Science. 2021;374:eabh2858.
41. Wang Y, DelRosso NV, Vaidyanathan TV, Cahill MK, Reitman ME, Pittolo S, et al. Accurate quantification of astrocyte and neurotransmitter fluorescence dynamics for single-cell and population-level physiology. Nat Neurosci. 2019;22:1936–44.
42. Wu Z, Cui Y, Wang H, Wu H, Wan Y, Li B, et al. Neuronal activity-induced, equilibrative nucleoside transporter-dependent, somatodendritic adenosine release revealed by a GRAB sensor. Proc Natl Acad Sci USA. 2023;120:e2212387120.
43. Badimon A, Strasburger HJ, Ayata P, Chen X, Nair A, Ikegami A, et al. Negative feedback control of neuronal activity by microglia. Nature. 2020;586:417–23.
44. Peng W, Wu Z, Song K, Zhang S, Li Y, Xu M. Regulation of sleep homeostasis mediator adenosine by basal forebrain glutamatergic neurons. Science. 2020;369:eabb0556.
45. Dosch M, Gerber J, Jebbawi F, Beldi G. Mechanisms of ATP Release by Inflammatory Cells. Int J Mol Sci. 2018;19:1222.
46. Xiong Y, Sun S, Teng S, Jin M, Zhou Z. Ca(2+)-Dependent and Ca(2+)-Independent ATP Release in Astrocytes. Front Mol Neurosci. 2018;11:224.
47. Schiavo G, Benfenati F, Poulain B, Rossetto O, Polverino de Laureto P, DasGupta BR, et al. Tetanus and botulinum-B neurotoxins block neurotransmitter release by proteolytic cleavage of synaptobrevin. Nature. 1992;359:832–5.
48. Li Y, Foran P, Fairweather NF, de Paiva A, Weller U, Dougan G, et al. A single mutation in the recombinant light chain of tetanus toxin abolishes its proteolytic activity and removes the toxicity seen after reconstitution with native heavy chain. Biochemistry. 1994;33:7014–20.
49. Sawada K, Echigo N, Juge N, Miyaji T, Otsuka M, Omote H, et al. Identification of a vesicular nucleotide transporter. Proc Natl Acad Sci USA. 2008;105:5683–6.
50. Oya M, Kitaguchi T, Yanagihara Y, Numano R, Kakeyama M, Ikematsu K, et al. Vesicular nucleotide transporter is involved in ATP storage of secretory lysosomes in astrocytes. Biochem Biophys Res Commun. 2013;438:145–51.
51. Shinozaki Y, Nomura M, Iwatsuki K, Moriyama Y, Gachet C, Koizumi S. Microglia trigger astrocyte-mediated neuroprotection via purinergic gliotransmission. Sci Rep. 2014;4:4329.
52. Covelo A, Araque A. Neuronal activity determines distinct gliotransmitter release from a single astrocyte. Elife. 2018;7:e32237.
53. Aggarwal A, Liu R, Chen Y, Ralowicz AJ, Bergerson SJ, Tomaska F, et al. Glutamate indicators with improved activation kinetics and localization for imaging synaptic transmission. Nat Methods. 2023;20:925–34.
54. Matejuk A, Ransohoff RM. Crosstalk Between Astrocytes and Microglia: An Overview. Front Immunol. 2020;11:1416.
55. Umpierre AD, Bystrom LL, Ying Y, Liu YU, Worrell G, Wu LJ. Microglial calcium signaling is attuned to neuronal activity in awake mice. Elife. 2020;9:e56502.
56. Li Q, Barres BA. Microglia and macrophages in brain homeostasis and disease. Nat Rev Immunol. 2018;18:225–42.
57. Imura Y, Morizawa Y, Komatsu R, Shibata K, Shinozaki Y, Kasai H, et al. Microglia release ATP by exocytosis. Glia. 2013;61:1320–30.
58. Huang Y, Xu Z, Xiong S, Sun F, Qin G, Hu G, et al. Repopulated microglia are solely derived from the proliferation of residual microglia after acute depletion. Nat Neurosci. 2018;21:530–40.

59. Hu NY, Chen YT, Wang Q, Jie W, Liu YS, You QL, et al. Expression Patterns of Inducible Cre Recombinase Driven by Differential Astrocyte-Specific Promoters in Transgenic Mouse Lines. Neurosci Bull. 2020;36:530–44.

60. Davalos D, Grutzendler J, Yang G, Kim JV, Zuo Y, Jung S, et al. ATP mediates rapid microglial response to local brain injury in vivo. Nat Neurosci. 2005;8:752–8.

61. Illes P, Rubini P, Ulrich H, Zhao Y, Tang Y. Regulation of Microglial Functions by Purinergic Mechanisms in the Healthy and Diseased CNS. Cells. 2020;9:1108.

62. Kyrargyri V, Madry C, Rifat A, Arancibia-Carcamo IL, Jones SP, Chan VTT, et al. P2Y(13) receptors regulate microglial morphology, surveillance, and resting levels of interleukin 1β release. Glia. 2020;68:328–44.

63. Haynes SE, Hollopeter G, Yang G, Kurpius D, Dailey ME, Gan WB, et al. The P2Y12 receptor regulates microglial activation by extracellular nucleotides. Nat Neurosci. 2006;9:1512–9.

64. Lin R, Zhou Y, Yan T, Wang R, Li H, Wu Z, et al. Directed evolution of adeno-associated virus for efficient gene delivery to microglia. Nat Methods. 2022;19:976–85.

65. Streit WJ, Mrak RE, Griffin WS. Microglia and neuroinflammation: a pathological perspective. J Neuroinflammation. 2004;1:14.

66. Colombo E, Farina C. Astrocytes: Key Regulators of Neuroinflammation. Trends Immunol. 2016;37:608–20.

67. Wei C, Jiang W, Wang R, Zhong H, He H, Gao X, et al. Brain endothelial GSDMD activation mediates inflammatory BBB breakdown. Nature. 2024;629:893–900.

68. Jourdain P, Bergersen LH, Bhaukaurally K, Bezzi P, Santello M, Domercq M, et al. Glutamate exocytosis from astrocytes controls synaptic strength. Nat Neurosci. 2007;10:331–9.

69. Cao X, Li LP, Wang Q, Wu Q, Hu HH, Zhang M, et al. Astrocyte-derived ATP modulates depressive-like behaviors. Nat Med. 2013;19:773–7.

70. Cho WH, Noh K, Lee BH, Barcelon E, Jun SB, Park HY, et al. Hippocampal astrocytes modulate anxiety-like behavior. Nat Commun. 2022;13:6536.

71. Lin S, Huang L, Luo ZC, Li X, Jin SY, Du ZJ, et al. The ATP Level in the Medial Prefrontal Cortex Regulates Depressive-like Behavior via the Medial Prefrontal Cortex-Lateral Habenula Pathway. Biol Psychiatry. 2022;92:179–92.

72. Luo L. Principles of Neurobiology, 2nd ed. New York: Garland Science; 2020.

73. Verkhratsky A, Matteoli M, Parpura V, Mothet JP, Zorec R. Astrocytes as secretory cells of the central nervous system: idiosyncrasies of vesicular secretion. Embo j. 2016;35:239–57.

74. Pryazhnikov E, Khiroug L. Sub-micromolar increase in [Ca(2+)](i) triggers delayed exocytosis of ATP in cultured astrocytes. Glia. 2008;56:38–49.

75. Jaiswal JK, Andrews NW, Simon SM. Membrane proximal lysosomes are the major vesicles responsible for calcium-dependent exocytosis in nonsecretory cells. J Cell Biol. 2002;159:625–35.

76. Xu H, Ren D. Lysosomal physiology. Annu Rev Physiol. 2015;77:57–80.

77. Upmanyu N, Jin J, Emde HV, Ganzella M, Bösche L, Malviya VN, et al. Colocalization of different neurotransmitter transporters on synaptic vesicles is sparse except for VGLUT1 and ZnT3. Neuron. 2022;110:1483–97.e7.

78. Allen NJ. Astrocyte regulation of synaptic behavior. Annu Rev Cell Dev Biol. 2014;30:439–63.

79. Xiong Y, Teng S, Zheng L, Sun S, Li J, Guo N, et al. Stretch-induced Ca(2+) independent ATP release in hippocampal astrocytes. J Physiol. 2018;596:1931–47.

80. Orellana JA, Froger N, Ezan P, Jiang JX, Bennett MV, Naus CC, et al. ATP and glutamate released via astroglial connexin 43 hemichannels mediate neuronal death through activation of pannexin 1 hemichannels. J Neurochem. 2011;118:826–40.

81. Chen Y, Luan P, Liu J, Wei Y, Wang C, Wu R, et al. Spatiotemporally selective astrocytic ATP dynamics encode injury information sensed by microglia following brain injury in mice. Nat Neurosci. 2024;27:1522–33.

82. Zhang Y, Chen K, Sloan SA, Bennett ML, Scholze AR, O'Keeffe S, et al. An RNA-sequencing transcriptome and splicing database of glia, neurons, and vascular cells of the cerebral cortex. J Neurosci. 2014;34:11929–47.

83. Kinoshita M, Hirayama Y, Fujishita K, Shibata K, Shinozaki Y, Shigetomi E, et al. Anti-Depressant Fluoxetine Reveals its Therapeutic Effect Via Astrocytes. EBioMedicine. 2018;32:72–83.

84. Kasymov V, Larina O, Castaldo C, Marina N, Patrushev M, Kasparov S, et al. Differential sensitivity of brainstem versus cortical astrocytes to changes in pH reveals functional regional specialization of astroglia. J Neurosci. 2013;33:435–41.

85. Beckel JM, Gómez NM, Lu W, Campagno KE, Nabet B, Albalawi F, et al. Stimulation of TLR3 triggers release of lysosomal ATP in astrocytes and epithelial cells that requires TRPML1 channels. Sci Rep. 2018;8:5726.

86. Li D, Hérault K, Silm K, Evrard A, Wojcik S, Oheim M, et al. Lack of evidence for vesicular glutamate transporter expression in mouse astrocytes. J Neurosci. 2013;33:4434–55.

87. Ma C, Li B, Silverman D, Ding X, Li A, Xiao C, et al. Microglia Regulate Sleep via Calcium-Dependent Modulation of Norepinephrine Transmission. Nat Neurosci. 2024;27:249–58.

88. Wheeler MA, Clark IC, Lee HG, Li Z, Linnerbauer M, Rone JM, et al. Droplet-based forward genetic screening of astrocyte-microglia cross-talk. Science. 2023;379:1023–30.

89. Liddelow SA, Guttenplan KA, Clarke LE, Bennett FC, Bohlen CJ, Schirmer L, et al. Neurotoxic reactive astrocytes are induced by activated microglia. Nature. 2017;541:481–7.

90. Guttenplan KA, Weigel MK, Prakash P, Wijewardhane PR, Hasel P, Rufen-Blanchette U, et al. Neurotoxic reactive astrocytes induce cell death via saturated lipids. Nature. 2021;599:102–7.

91. Ramamoorthy P, Whim MD. Trafficking and fusion of neuropeptide Y-containing dense-core granules in astrocytes. J Neurosci. 2008;28:13815–27.

92. Schwarz Y, Zhao N, Kirchhoff F, Bruns D. Astrocytes control synaptic strength by two distinct v-SNARE-dependent release pathways. Nat Neurosci. 2017;20:1529–39.

93. Wang H, Qian T, Zhao Y, Zhuo Y, Wu C, Osakada T, et al. A tool kit of highly selective and sensitive genetically encoded neuropeptide sensors. Science. 2023;382:eabq8173.

94. Lin R, Liang J, Wang R, Yan T, Zhou Y, Liu Y, et al. The Raphe Dopamine System Controls the Expression of Incentive Memory. Neuron. 2020;106:498–514.e8.

AUTHOR CONTRIBUTIONS
HL and ML conceived the study. ML supervised the project. HL performed surgeries, imaging, immunostaining, smFISH, and data analysis. YZ helped to perform surgeries and process data. PG performed RT-qPCR. RD, DW, FY, WW, and RL contributed to plasmid cloning and AAV packaging. YL and ZW provided GRAB sensors and the VNUT floxed mouse line. HL drafted the figures. HL and ML wrote the manuscript with inputs from all authors.

COMPETING INTERESTS
The authors declare no competing interests.

ADDITIONAL INFORMATION
Supplementary information The online version contains supplementary material available at https://doi.org/10.1038/s41380-024-02851-8.

Correspondence and requests for materials should be addressed to Minmin Luo.

Reprints and permission information is available at http://www.nature.com/reprints

Publisher's note Springer Nature remains neutral with regard to jurisdictional claims in published maps and institutional affiliations.